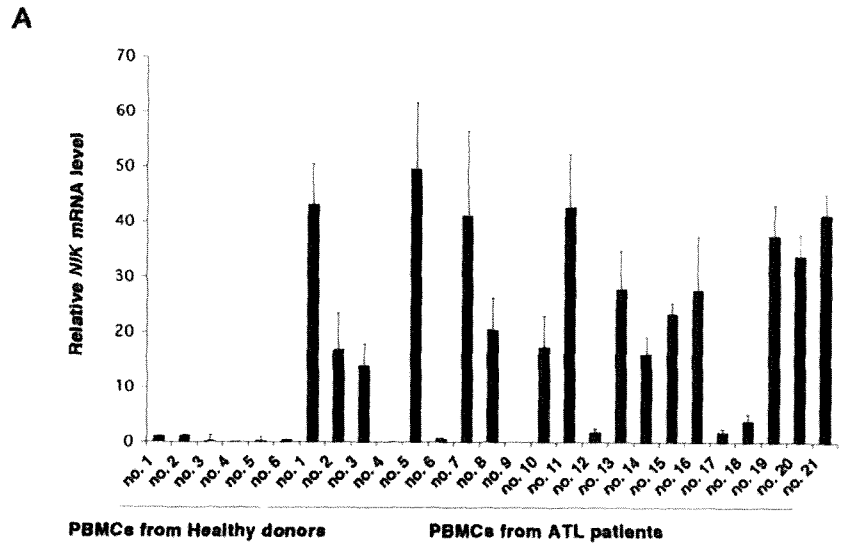

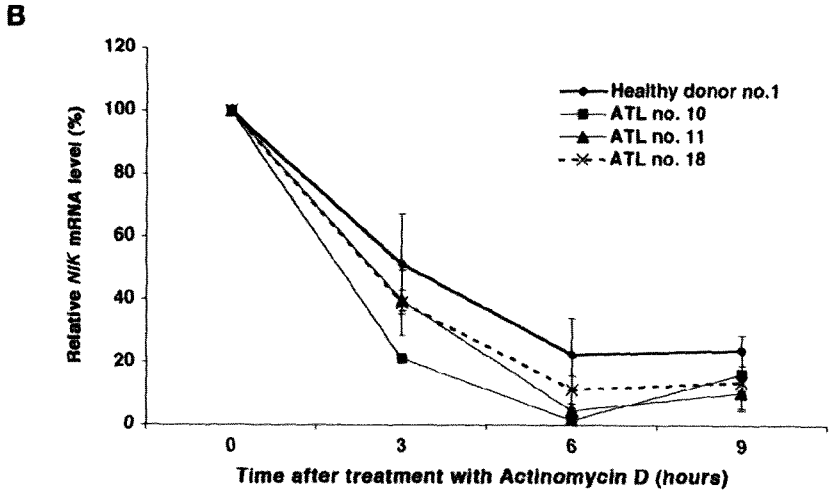

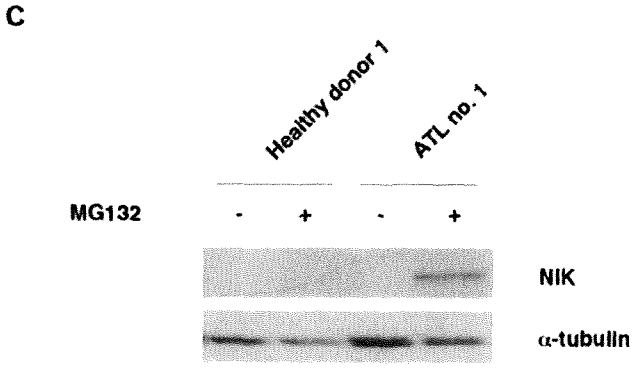

Figure 2. Overexpression of the *NIK* mRNA and protein in PBMCs from ATL patients. (A) Total RNA was extracted from PBMCs from healthy donors and ATL patients and then subjected to quantitative RT-PCR. The *NIK* mRNA levels were normalized to *18S* RNA. The relative *nik* mRNA levels shown represent the fold increases in mRNA abundance relative to that of healthy donor 1 (arbitrarily set at 1). These data are expressed as the mean plus or minus SD of 3 independent experiments. (B) PBMCs were cultured in the presence of actinomycin D (5 μg/mL) for the times indicated, and then total RNA was isolated and subjected to quantitative RT-PCR. The relative amounts of *NIK* mRNA shown represent the percentages in mRNA abundance, relative to that of PBMCs before the addition of actinomycin D (arbitrarily set at 100%). (C) PBMCs from a healthy donor and an ATL patient were treated with (+) or without (−) MG132 (20 μM) for 3 hours, lysed with RIPA buffer, and subjected to immunoblotting with anti-NIK or anti-α-tubulin antibodies.

expressed this protein (Figure 3A) without significant morphologic change (Figure 5B) or constitutive NF-κB activation (Figure 3C). As expected, these cells failed to survive selection with blasticidin S (data not shown).

The expression of wild-type NIK in B5 and h12 cells potently induces p52 expression and NF-κB DNA binding activity, whereas the catalytically inactive NIK mutant does not (Figure 3B,C). We also found a specifically phosphorylated form of IκBα in cells expressing wild-type NIK (Figure 3A). Super-shift experiments revealed that the NF-κB–DNA binding complexes in B5 and h12 cells expressing NIK involve p50, RelB, and RelA (Figure 4D). The presence of p52 in the DNA binding complexes could not be examined, however, because an antibody recognizing rat p52 in super-shift assay is not currently available. Instead, we analyzed DNA-binding complexes induced by NIK expression in wild-type mouse embryonic fibroblasts (Figure S2). Retroviral overexpression of NIK indeed induced DNA-binding NF-κB complexes containing p52, and enhanced expression of p52 and phosphorylated form of IκBα.

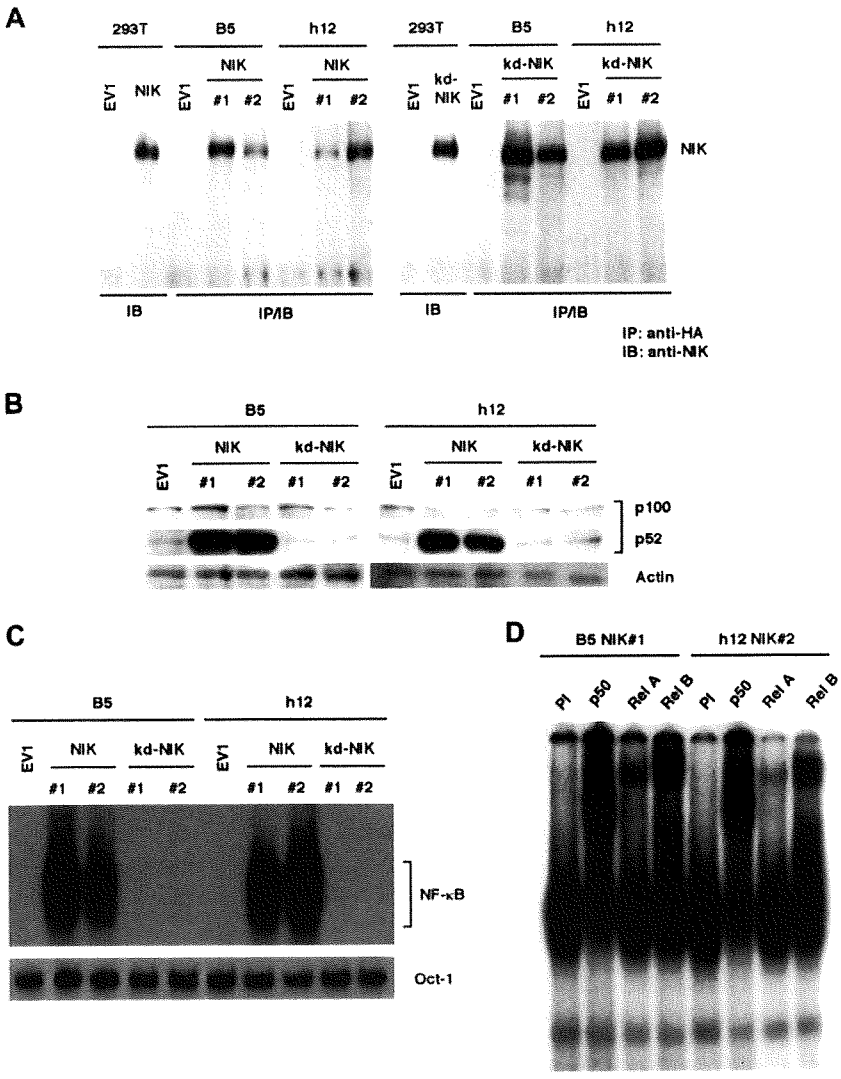

Figure 3. NIK induces constitutive NF-κB activity in rat fibroblasts. (A) B5 and h12 cells were infected with retroviruses capable of expressing HA-tagged NIK (NIK) or catalytically inactive NIK (kd-NIK). Pools of B5 and h12 cells transduced with the control pMRX-HAiresPuro vector (EV1) were used as a control. Cytoplasmic extracts from EV1 and 2 independent cell clones (no. 1 and no. 2) were subjected to immunoprecipitation using antibody against the HA epitope. Immunoprecipitates were then resolved by 8% SDS-PAGE and subjected to immunoblotting with anti-NIK antibody. 293T cells were transiently transfected with the pMRX-HAiresPuro vector (EV1) or pMRX-HA-NIKiresPuro (NIK). Cytoplasmic extracts (30 μg) were then used for immunoblotting as negative and positive controls, respectively. (B) Elevated p52 production in rat fibroblasts. Whole-cell lysates from B5 and h12 cells expressing wild-type NIK or kd-NIK were subjected to SDS-PAGE and immunoblotting with anti-p52 for detection of p100 and p52 or antiactin antibodies. (C) Elevated NF-κB–DNA binding activity in rat fibroblasts; 5 μg of nuclear extracts prepared from B5 and h12 cells expressing wild-type NIK or kd-NIK were analyzed by EMSA, using oligonucleotides encoding an NF-κB–binding sequence or Oct-1–binding sequence as probes. (D) DNA-binding NF-κB components in B5 and h12 cells expressing wild-type NIK were analyzed by super-shift EMSA. Nuclear extracts (5 μg) from B5 NIK#1 and h12 NIK#2 cells were preincubated for 30 minutes with preimmune (PI), anti-p50, anti-RelA or anti-RelB sera, and then subjected to EMSA with the NF-κB–specific probe. IB indicates immunoblotting; IP, immunoprecipitation.

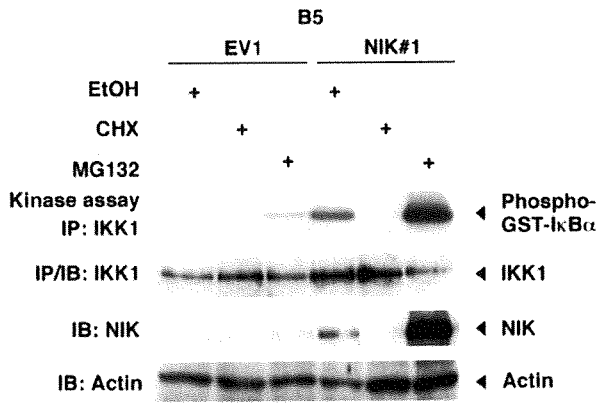

Figure 4. NIK expression parallels IKK activity after CHX or MG132 treatment. B5 cells transduced with the control vector (EV1) or B5 cells expressing wild-type NIK (NIK#1) were treated for 4 hours with either vehicle (ethanol, EtOH), cycloheximide (CHX; 50 μg/mL), or MG132 (20 μM). Cytoplasmic extracts were subjected to immunoprecipitation with IKK1-specific antibody, and then immunoprecipitates were used for an in vitro kinase assay. IKK1 expression in the immunoprecipitates was revealed by immunoblotting with IKK1-specific antibody. NIK and actin levels in the cytoplasmic extracts used for immunoprecipitation were determined by immunoblotting with anti-NIK or antiactin antibodies, respectively. IB indicates immunoblotting; IP, immunoprecipitation; GST, glutathione-S-transferase tag.

We have previously demonstrated that the treatment of ATL cells with MG132 greatly enhances IKK activity, whereas protein synthesis inhibition quickly abolished this activity.[11] Figure 4 shows that the IKK activity in B5 cells stably expressing NIK (NIK#1) is modulated by MG132 and cycloheximide (CHX) in a manner that is very similar to that seen in ATL cells. In addition, treatment of NIK#1 cells with MG132 remarkably elevates the level of exogenous NIK expression. The constitutive NF-κB activation caused by the presence of exogenous NIK was found to be abolished by the retroviral expression of a super-repressor form of IκBα (SR-IκBα), without affecting exogenous NIK expression (Figure 5A). Interestingly, the forced expression of SR-IκBα also diminishes the p52 and p100 expression levels.

We next tested the ability of NIK to induce anchorage-independent growth of rat fibroblasts. B5 and h12 cells transduced with the control vector did not form colonies of significant size in soft agar, whereas those transduced with wild-type NIK expression vector formed a number of large colonies, as shown in Figure 5B and Table 1. Cells expressing catalytically inactive NIK failed to form colonies in soft agar. The expression of SR-IκBα completely abolished NIK-induced colony formation and also the morphologic alterations of B5 and h12 cells. Given that SR-IκBα specifically suppresses NF-κB activation,

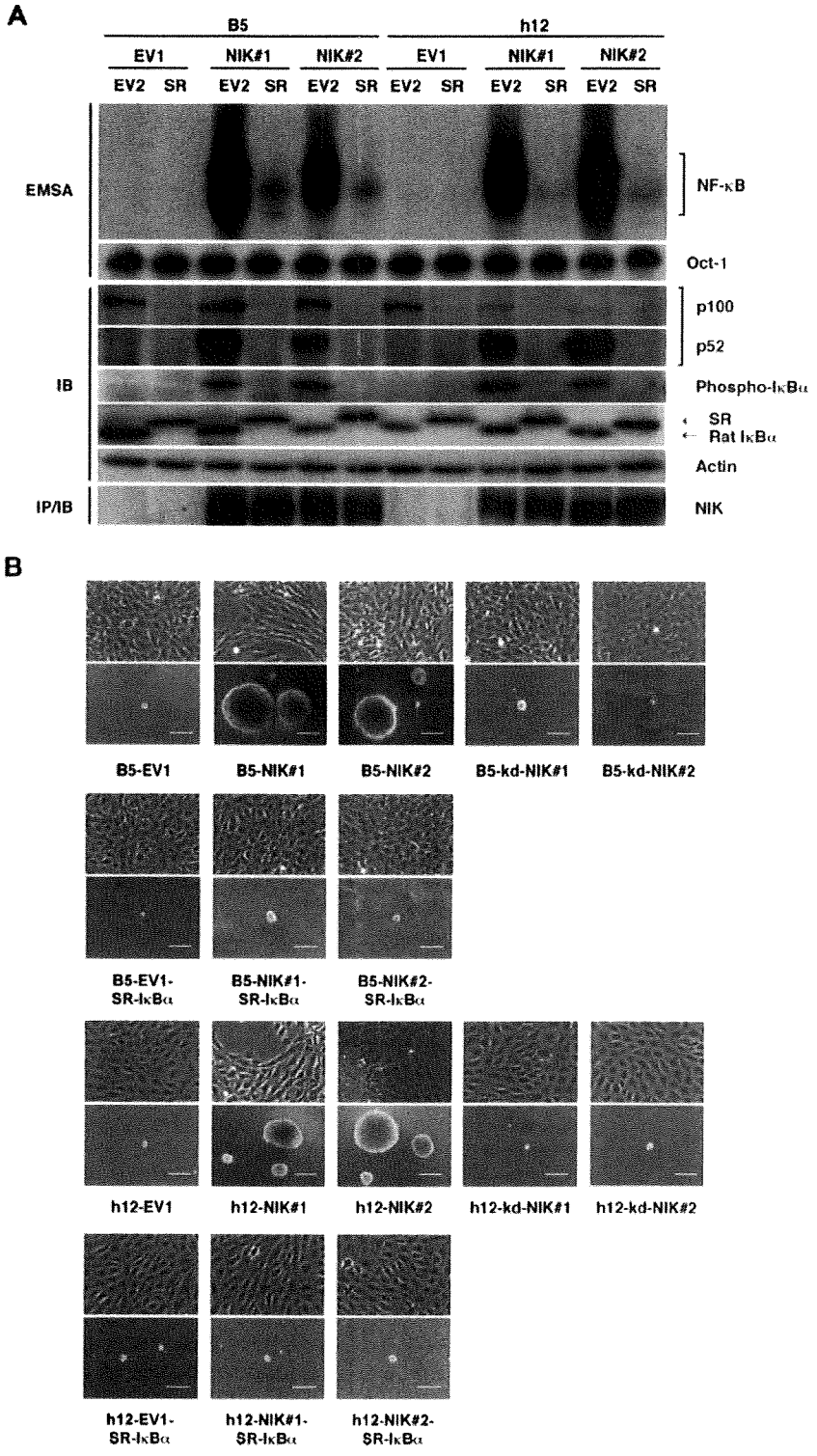

Figure 5. The overexpression of NIK transforms rat fibroblasts in an NF-κB–dependent manner. (A) Top 2 panels: 5 μg of nuclear extracts prepared from B5 and h12 cells transduced with empty vector (EV2) or SR-IκBα (SR) were analyzed by EMSA, using NF-κB and Oct-1 probes. Middle 5 panels: whole-cell extracts (30 μg) of B5 or h12 infectants were subjected to SDS-PAGE and immunoblotting with anti-p52, antiphospho-IκBα, anti-IκBα, or antiactin antibodies. Bottom panel: HA-tagged NIK was immunoprecipitated from B5 and h12 infectants with anti-HA antibody and detected by immunoblotting with anti-NIK antibody (H-248). (B) Phase-contrast micrographs of cells cultured on monolayers (top images) or in soft agar (bottom images). B5 or h12 cell clones expressing wild-type NIK (NIK#1 and NIK#2) or not (EV1) were cultured in soft agar for 3 weeks. These cells were further transduced with SR-IκBα, and then pooled cells were assayed for anchorage-independent growth in soft agar. B5 and h12 cell clones expressing kd-NIK were also examined. Original magnification 100. Scale bar represents 100 μm. SR indicates super-repressor; kd-NIK, catalytically inactive NIK; IB, immunoblotting; IP, immunoprecipitation.

we conclude from these results that NIK transforms rat fibroblasts in an NF-κB–dependent manner.

NIK mediates constitutive NF-κB activation in ATL cells

The similar modulation of IKK activity by CHX or MG132 in both ATL and B5 cells expressing NIK (Figure 4) suggests that NIK plays an important role in constitutive NF-κB activation in ATL cells. We therefore examined whether the RNA interference-mediated silencing of endogenous *NIK* gene expression would lower NF-κB–dependent transcription in these cells. ED-40515(−) and ATL-43Tb(−) cells were infected with lentiviral constructs that express short hairpin RNA (shRNA) molecules that target mRNA for either *Renilla luciferase* (Ctli) or *NIK* (NIKi), and then subjected to puromycin selection for 2 days. To

Table 1. Efficiency of colony formation in soft agar

Cells*	Colony-forming efficiency, %	Average size of colonies, μm†
B5-EV1	0.7 ± 0.5	62.6 ± 1.5
B5-NIK#1	23.2 ± 2.0‡	236.2 ± 12.6‡
B5-NIK#2	18.9 ± 2.4‡	184.1 ± 19.8‡
B5-kd-NIK#1	1.5 ± 0.3	63.1 ± 1.4
B5-kd-NIK#2	1.3 ± 0.1	62.8 ± 1.8
h12-EV1	1.2 ± 0.3	60.5 ± 0.0
h12-NIK#1	12.8 ± 1.7‡	146.9 ± 4.6‡
h12-NIK#2	17.7 ± 1.7‡	154.9 ± 5.6‡
h12-kd-NIK#1	1.4 ± 1.0	61.5 ± 2.1
h12-kd-NIK#2	1.5 ± 0.4	62.5 ± 4.7
B5-EV1-EV2	1.2 ± 0.3	61.8 ± 1.1
B5-NIK#1-EV2	21.1 ± 1.0‡	193.8 ± 3.7‡
B5-NIK#2-EV2	14.3 ± 1.0‡	150.4 ± 8.7‡
h12-EV1-EV2	1.5 ± 0.7	60.8 ± 0.4
h12-NIK#1-EV2	12.3 ± 1.7‡	119.4 ± 5.6‡
h12-NIK#2-EV2	14.0 ± 1.8‡	160.3 ± 7.2‡
B5-EV1-SR-IκBα	1.5 ± 0.0	61.7 ± 0.5
B5-NIK#1-SR-IκBα	3.4 ± 0.0	64.8 ± 1.1
B5-NIK#2-SR-IκBα	3.9 ± 0.1	63.3 ± 0.4
h12-EV1-SR-IκBα	1.7 ± 1.0	61.3 ± 0.4
h12-NIK#1-SR-IκBα	2.7 ± 0.3	62.3 ± 0.1
h12-NIK#2-SR-IκBα	3.4 ± 1.4	61.4 ± 0.2

kd-NIK indicates catalytically inactive NIK; SR, super-repressor; EV1, empty vector for NIK or kd-NIK; and EV2, empty vector for SR-IκBα.

*Cells were inoculated in 0.33% soft agar and cultured for 3 weeks.

†Colonies larger than 60 μm were counted as positive. The sizes of more than 100 positive colonies were averaged.

‡$P < .05$ vs B5-EV1.

suppress NIK expression maximally, we used independently or in combination 2 shRNAs (NIKi-1 and -2) that target different *NIK* sequences and reduce NIK expression. The infected cells were then assayed for transcriptional activity by transient transfection with an NF-κB–dependent reporter gene (Figure 6A). Lentiviral expression of NIKi constructs resulted in suppression of NF-κB–dependent reporter gene expression in ATL cells when independently used, and the combined use of the 2 NIKi constructs (NIKi-1 and -2) was found to be more effective. We then examined ATL cells transduced with NIKi-1 and -2 constructs for the expression of endogenous NIK and specifically phosphorylated forms of p100, IκBα, and IKKs by immunoblotting (Figure 6B) and for NF-κB DNA binding activity by EMSA (Figure 6C). NIK expression in ATL cells was found to be down-regulated by the shRNA-mediated silencing (Figure 6B). As expected, p52 and phosphorylated p100 were also reduced by NIK depletion, and interestingly, phoshorylation of IκBα was also suppressed. This is consistent with the results observed in NIK-transduced rat fibroblasts that express the phoshorylated form of IκBα (Figure 5A), indicating that NIK, when aberrantly and stably expressed, induces phosphorylation of IκBα. In addition, NIK depletion suppressed phosphorylation of the serine residues in the activation loop of IKKs, suggesting a key role for NIK in constitutive activation of IKKs in ATL cells (Figure 6B). Moreover, depletion of NIK resulted in suppression of NF-κB DNA binding activity (Figure 6C). Super-shift assays revealed that DNA-binding of NF-κB components, p50, p52, RelA, and RelB was reduced by NIK depletion (Figure 6D). As shown previously, c-Rel was not detected in ATL cells.[34] We further investigated alterations in the expression of NF-κB target genes by NIK depletion. Vascular endothelial growth factor (VEGF), matrix metalloproteinase-9 (MMP-9), and intracellular adhesion molecule-1 (ICAM-1), the expression of which has been reported to be under the control of NF-κB,[35-37] are highly expressed in ATL cells and suggested to contribute to their invasive properties.[38-41] Quantitative RT-PCR studies reveal that depletion of NIK results in down-regulation of the expression of these NF-κB target genes (Figure 6E).

NIK regulates tumorigenicity of ATL cells in vivo

We finally investigated biologic effects of NIK depletion in ATL cells. NIK depletion did not significantly influence the growth of cells in culture (Figure 7A). We then examined whether depletion of NIK affects the tumorigenicity of ATL cells in a mouse model. NOD/SCID/γc^{null} mice were subcutaneously inoculated with ED-40515(−) cells that express Ctli or NIKi and are characterized in Figure 6B,C, and tumor formation was evaluated 2 weeks later. As expected, ED-40515(−) cells expressing Ctli efficiently formed large tumors, whereas tumors formed in mice inoculated with ED-40515(−) cells expressing NIKi were significantly smaller (Figure 7B-D), suggesting that NIK supports efficient tumor cell growth in vivo.

Discussion

Persistent activation of NF-κB has previously been reported to play an essential role in the growth and survival of specific cancer cell types, including ATL, H-RS, melanoma, and prostate cancer cells.[9,42-45] Inappropriate NF-κB activation can also contribute to the resistance to the apoptotic responses induced by certain anticancer drugs.[46] On the other hand, cancer cell apoptosis can be induced when persistent NF-κB activity is blocked by inhibitors, such as SR-IκBα, by drugs targeting IKK or the proteasome, via peptides targeting p50 or NEMO, and by double-stranded oligonucleotides containing NF-κB binding sites.[47,48] One problem with such inhibitors, however, is their lack of specificity to cancer cells because they also necessarily block normal NF-κB activation. Hence, it would be desirable to specifically inhibit NF-κB activation in cancer cells by identifying molecular targets in each cancer type. Virally transformed cancer cells express a virus-derived regulatory protein(s) that targets critical molecules in a variety of key signaling pathways. Cytokine autocrine loops or genetic alterations to genes regulating the NF-κB signaling mechanisms that lead to persistent NF-κB activation have also been identified in some cancer cells.[16,17,32,47,49] However, the mechanisms underlying persistent NF-κB activation in many types of cancer remain unknown.

Most primary ATL cells, although infected with HTLV-I, are characterized by the loss of viral protein expression, including Tax, probably because of the host immune surveillance during the long period of latency.[50] Nevertheless, NF-κB is strongly and persistently activated in ATL cells through IKK,[9] although the mechanism of IKK activation has remained unknown. The findings in our present study demonstrate the aberrant expression of *NIK* at the pretranslational level in ATL cells derived from 15 of 21 patients. This overexpression does not seem to correlate with the patients' age, sex, disease type, or percentage of abnormal lymphocytes (Table S1). Further studies will be required to clarify potentially NIK-independent NF-κB activation in the other 6 cases. The stable expression of functional NIK in fibroblasts, but not that of its catalytically inactive mutant, causes cellular transformation and persistent NF-κB activation with molecular features quite similar to those reported previously in ATL cells. These include the rapid

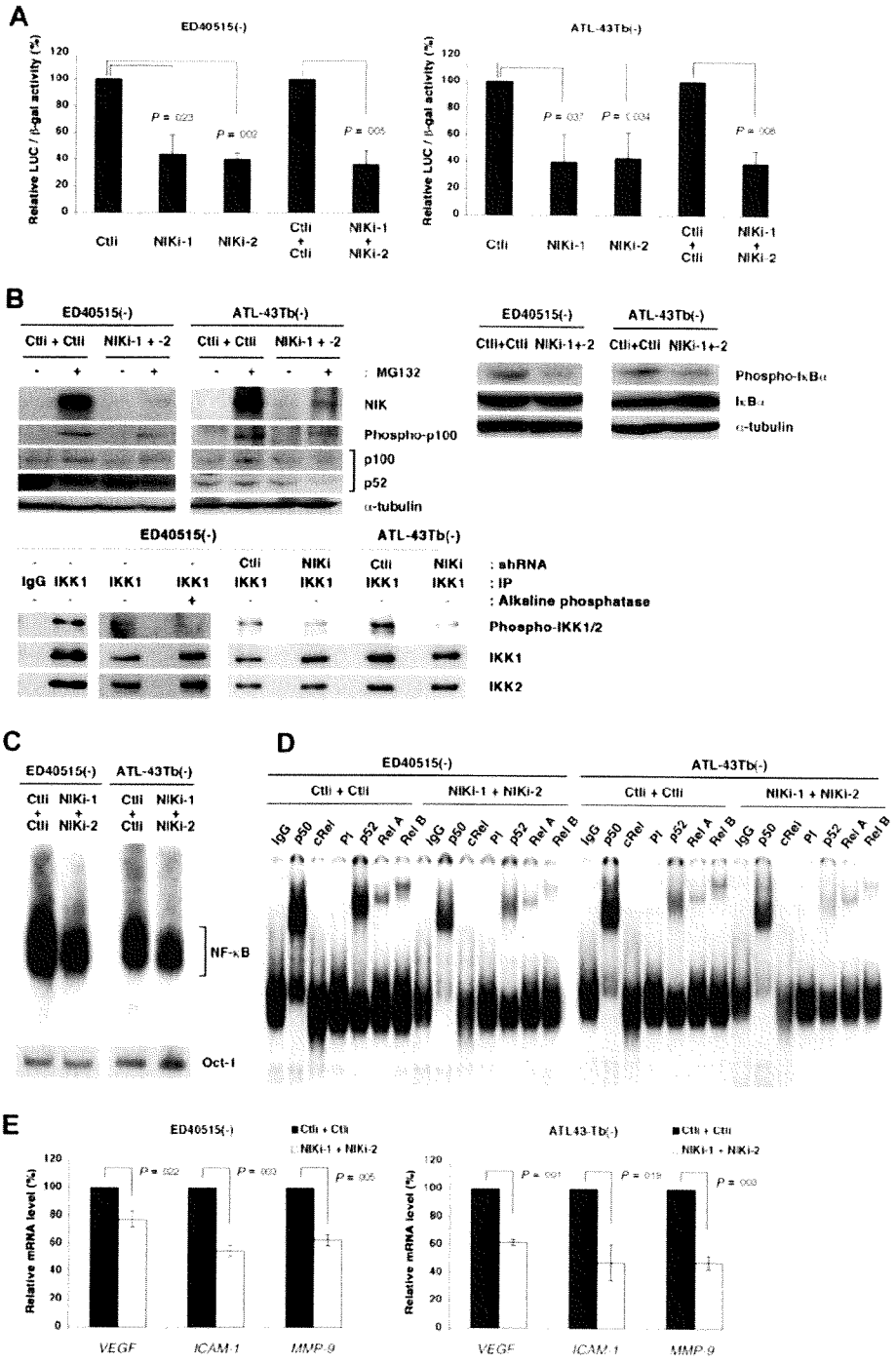

Figure 6. Depletion of NIK suppresses NF-κB-dependent transcription in ATL cells. (A) ED40515(−) and ATL-43Tb(−) cells were infected with lentiviral vectors expressing *Renilla luciferase* (Ctli) or *NIK*-specific shRNAs (NIKi-1 or NIKi-2). In parallel, ED40515(−) and ATL-43Tb(−) cells were infected with lentiviral vectors expressing Ctli or NIKi-1 shRNAs, and 24 hours later, these cells were super-infected with lentiviral vectors expressing Ctli or NIKi-2 shRNAs. Twenty-four hours after infection, cells were selected with puromycin for 2 days. Puromycin-resistant cells were then transfected with 2 μg of IgκCona-Luc and 2 μg EF1-LacZ. Luciferase (LUC) activity was determined 48 hours after transfection and normalized to β-gal activity. Relative luciferase activities, in comparison with control cells, 100 are shown. Data are expressed as mean plus or minus SD of 3 independent experiments. *P* values are versus control (Ctli). (B) Super-infected cells were treated with or without MG132 (20 μM) for 3 hours and subjected to SDS-PAGE and immunoblotting with anti-NIK (#4994), antiphosphorylated p100, or anti-α-tubulin antibodies. Whole-cell extracts (30 μg) from these cells were analyzed by SDS-PAGE and immunoblotting with antiphospho-IκBα, anti-IκBα, or anti-α-tubulin antibodies. Cytoplasmic extracts prepared from ED40515(−) cells infected or not with lentivirus were precleared and immunoprecipitation was performed, using anti-IKK1 monolconal antibody or its isotype IgG (IgG). After 3 washes with TNT buffer, immune complexes were treated or not with Shrimp Akaline Phosphatase (Takara Bio) and then subjected to SDS-PAGE and immunoblotting with antiphospho-IKK1/2, anti-IKK1, or anti-IKK2 antibodies. (C) A total of 5 μg of nuclear extracts prepared from lentivirus-infected cells shown in panel B were analyzed by EMSA, using oligonucleotides encoding the NF-κB–binding sequence or Oct-1–binding sequence as probes. (D) Nuclear extracts (5 μg) from lentivirus-infected cells shown in panel B were preincubated for 30 minutes with purified mouse IgG, anti-p50, anti-cRel antibody, preimmune (PI), anti-p50, anti-RelA or anti-RelB sera, and then subjected to EMSA with the NF-κB–specific probe. (E) Total RNAs from lentivirus-infected cells shown in panel B were examined by quantitative RT-PCR for *VEGF*, *ICAM-1*, and *MMP-9* mRNA levels. Each mRNA level was normalized to *18S* RNA. Relative mRNA levels, in comparison with control cells, 100 are shown. Data are expressed as mean plus or minus SD of 3 independent experiments. *P* values are versus control (Ctli + Ctli).

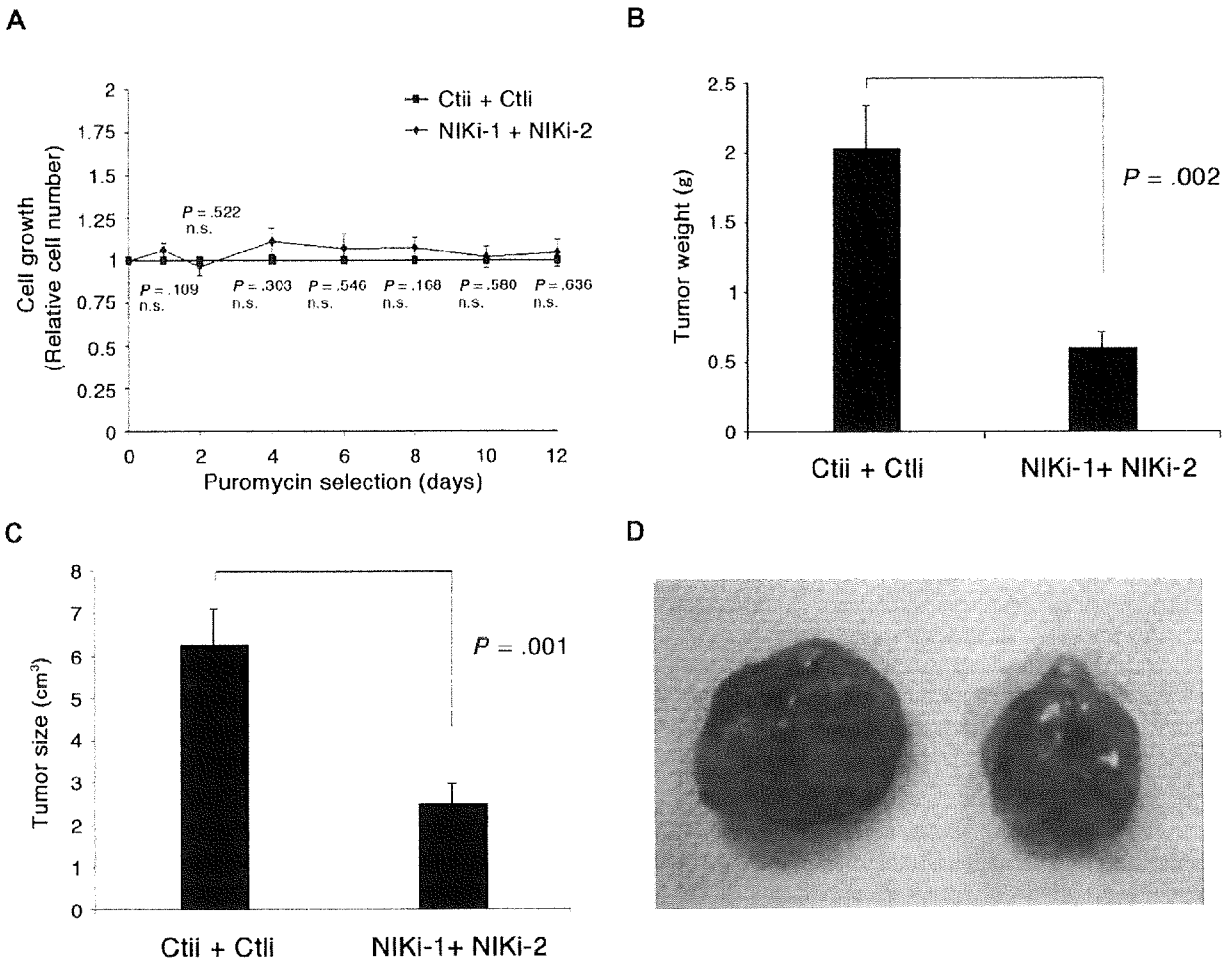

Figure 7. Depletion of NIK in ATL cells suppresses tumor formation in NOD-SCID/γc^{null} (NOG) mice. (A) Pools of ED40515(−) cells expressing Ctli or NIKi-1 and -2, shown in Figure 6B, C, D, and E, were analyzed for cell growth in vitro by the trypan blue staining method. Relative cell numbers, in comparison with control cells (arbitrarily set at 1), are shown. Data are expressed as mean plus or minus SD of 3 independent experiments. *P* values are vs control (Ctli + Ctli). n.s. indicates no significant difference. (B-D) NOG mice were inoculated subcutaneously in the postauricular region with the puromycin-resistant ED-40515(−) cells (5 10^6). Tumor formation in mice was evaluated 2 weeks after inoculation. Tumor weight (B) and size (C) relative to those of tumors formed in mice inoculated with ED40515(−) cells expressing Ctli are shown. (D) Photographs of tumors formed 2 weeks after cell inoculation. Each result was obtained from 5 different mice (means are shown [error bars]). *P* values are versus control (Ctli + Ctli).

loss of IKK activity after protein synthesis inhibition and the superinduction of IKK activity in the presence of MG132.[11] Moreover, RNA interference studies have also indicated that the deregulated NIK expression is the principal cause of constitutive NF-κB activation in ATL cells. In line with a previous report by Ramakrishnan et al, which showed that the induction of IκBα degradation by CD70, CD40 ligand, and BLyS/BAFF is dependent on the function of NIK,[18] we find in our present experiments that the stable expression of NIK induces IκBα phosphorylation and the formation of DNA binding complexes containing not only p50 and RelB, but also RelA both in wild-type and in NEMO-deficient rat fibroblasts. This indicates that NIK can stimulate the canonical pathway characterized by IκBα phosphorylation and RelA activation and that NIK does not require NEMO for it. Interestingly, the forced expression of SR-IκBα in these fibroblasts abolishes the transformed phenotype and suppresses constitutive NF-κB activity, with the p100 and p52 expression levels being diminished simultaneously, probably because p100 expression is largely dependent on NF-κB activity.[51] RelB expression is also known to be controlled by NF-κB,[52] suggesting that the noncanonical pathway of NF-κB activation does not work independently but rather coincides with NF-κB activation through the canonical pathway under stable conditions.

H-RS cells were also found to overexpress NIK, including its transcripts, in this study. Earlier reports have described 2 potential mechanisms of constitutive NF-κB activation in H-RS cells: persistent signaling from receptors that cause NF-κB activation, such as CD30, CD40, and RANK as well as a CD40-like molecule latent membrane protein 1 of the Epstein-Barr virus; and disruption of IκBα-dependent suppression resulting from the mutation of this gene.[32,48] The H-RS cell lines used in this study are Epstein-Barr virus-negative, and neither HDLM-2 nor L540 cells harbor mutations in their *IκB* genes. Indeed, CD30, CD40, and RANK were all found to be expressed in the H-RS cell lines used in this study, but we envisage that the aberrant expression of NIK is a distinct mechanism underlying the persistent NF-κB activation in these cells. It is partly because these TNF family receptor molecules, when stimulated or overexpressed transiently in cultured cells, elevate the NIK protein expression levels with a concomitant reduction in TRAF3 but do not increase *NIK* mRNA.[19,20]

Whereas the transient stimulation of a B-cell line with BAFF or anti-CD40 antibody stabilizes the NIK protein at the posttranslational level and does not up-regulate its mRNA expression,[20] NIK was observed to be constitutively overexpressed in ATL and H-RS cells at the pretranslational level. These differing mechanisms of NIK regulation may not be all that surprising, however, in light of the transient vs persistent nature of the activation of NF-κB. The barely detectable levels of steady-state NIK protein expression and its robust accumulation after proteasome inhibition in ATL and H-RS cells further suggest that the proteasome-dependent degradation of NIK occurs rapidly in tumor cells as in normal cells, although we cannot rule out the possibility that TNF family receptors known to be overexpressed in H-RS cells influence the stability of NIK to some extent. This point is currently very difficult to address because the protein amount of NIK in the absence of the proteasome inhibitor is quite limited. At least 3 mechanisms of pretranslational induction of NIK are plausible: the stabilization of *NIK* transcripts, transcriptional activation and/or amplification of the *NIK* gene. It should be noted that the stability of *NIK* mRNA in ATL cells was similar to that in control cells, suggesting that NIK expression is deregulated in ATL cells at the level of mRNA production. In this regard, we are currently analyzing the regulatory region of the *NIK* gene in normal and cancer cells.

We detected NIK in whole-cell lysates only when the cells themselves were treated with the proteasome inhibitor, MG132. It is possible that the expression of the NIK protein is tightly regulated under detectable levels in resting normal cells. However, in ATL and H-RS cells, enhanced NIK production, although still not detectable by simple immunoblotting, may be sufficient to cause its deregulated activity toward IKK. During the manuscript preparation, 2 reports demonstrated deregulated expression of NIK because of mutations in *TRAF3*, *CYLD*, or *NIK* itself in multiple myeloma cells.[16,17] In case of ATL cells, formation of a fusion protein after genomic rearrangement seems to be unlikely based on the apparently normal size of the protein. At present, the mechanism of overproduction of *NIK* mRNA in ATL cells remains to be determined, but the fluorescence in situ hybridization results suggest that aberrant NIK expression in ATL cells is not the result of genomic abnormalities, such as amplification or translocation.

Successful anticancer drug or gene therapies can be conducted in a number of ways, including the general administration of particular reagents that mechanistically work exclusively on cancer cells, or delivering conventional anticancer reagents specifically to cancer cells. The former strategy is likely to be more promising in the case of hematopoietic cancers. In this regard, NIK could be an attractive molecular target for ATL and Hodgkin lymphoma therapy, although the physiologic functions of NIK in human adults remain unknown. Suppressing high NF-κB activity levels by targeting NIK may also sensitize these cancer cells to commonly used anticancer agents.

Acknowledgments

The authors thank all of the ATL patients who donated blood samples for use in this study, Dr K. Yamaguchi and the Joint Study on Predisposing Factors of ATL Development for providing and analyzing sample blood, and the following researchers for donating invaluable reagents: Dr M. Maeda (Kyoto University, Kyoto, Japan) for the ED40515(−) and ATL-43Tb(−) cells, Dr D. Goeddel (Amgen, Thousand Oaks, CA) for *NIK* cDNAs, Dr N.R. Rice and Dr A. Israël (Institut Pasteur Paris, Paris, France) for p50, RelA, and RelB antisera, Dr T. Kitamura (University of Tokyo, Tokyo, Japan) for Plat-E cells, Dr I.S.Y. Chen (UCLA, Los Angeles, CA) for pHCMV-VSVG and pCMVΔR8.2 packaging plasmids, and Dr H. Miyoshi (RIKEN Tsukuba Institute, Tsukuba, Japan) for CS-CDF-CG-PRE plasmid. The authors also thank Dr G. Courtois (INSERM, Paris, France) and the members of the Department of Molecular Virology for helpful discussions.

This work was supported by research grants from the Ministry of Health and Labor Sciences (HIV/AIDS, H18-005) (Naoki Yamamoto) and from the Ministry of Education, Culture, Sports, Science and Technology of Japan (18390145; Naoki Yamamoto) and (17013029; S.Y.).

Authorship

Contribution: Y.S., T.S., and S.Y. designed the study; Y.S., Norio Yamamoto, H.S., V.J.M.B., Y.I., K.M., X.Q., I.I., J.I., and S.Y. carried out the research; M.Z.D. carried out the animal experiments; A.U. and T.W. collected and analyzed sample blood from ATL patients; T.M. contributed to lentiviral vector constructions; Y.S. and S.Y. analyzed the data; T.S., Naoki Yamamoto and S.Y. controlled the data; Y.S. and S.Y. wrote the paper; all authors checked the final version of the manuscript.

Conflict-of-interest disclosure: The authors declare no competing financial interests.

Correspondence: Shoji Yamaoka, Department of Molecular Virology, Graduate School of Medicine, Tokyo Medical and Dental University, 1-5-45, Yushima, Bunkyo-ku, Tokyo, 113-8510, Japan; e-mail: shojmmb@tmd.ac.jp.

References

1. Baldwin AS Jr. Series introduction: the transcription factor NF-kappaB and human disease. J Clin Invest. 2001;107:3-6.
2. Hayden MS, Ghosh S. Signaling to NF-kappaB. Genes Dev. 2004;18:2195-2224.
3. Xiao G, Rabson AB, Young W, Qing G, Qu Z. Alternative pathways of NF-kappaB activation: a double-edged sword in health and disease. Cytokine Growth Factor Rev. 2006;17:281-293.
4. Coope HJ, Atkinson PG, Huhse B, et al. CD40 regulates the processing of NF-kappaB2 p100 to p52. EMBO J. 2002;21:5375-5385.
5. Claudio E, Brown K, Park S, Wang H, Siebenlist U. BAFF-induced NEMO-independent processing of NF-kappa B2 in maturing B cells. Nat Immunol. 2002;3:958-965.
6. Karin M, Cao Y, Greten FR, Li ZW. NF-kappaB in cancer: from innocent bystander to major culprit. Nat Rev Cancer. 2002;2:301-310.
7. Jost PJ, Ruland J. Aberrant NF-{kappa}B signaling in lymphoma: mechanisms, consequences and therapeutic implications. Blood. 2006;109:2700-2707.
8. Ni H, Ergin M, Huang Q, et al. Analysis of expression of nuclear factor kappa B (NF-kappa B) in multiple myeloma: downregulation of NF-kappa B induces apoptosis. Br J Haematol. 2001;115:279-286.
9. Hironaka N, Mochida K, Mori N, Maeda M, Yamamoto N, Yamaoka S. Tax-independent constitutive IkappaB kinase activation in adult T-cell leukemia cells. Neoplasia. 2004;6:266-278.
10. Nonaka M, Horie R, Itoh K, Watanabe T, Yamamoto N, Yamaoka S. Aberrant NF-kappaB2/p52 expression in Hodgkin/Reed-Sternberg cells and CD30-transformed rat fibroblasts. Oncogene. 2005;24:3976-3986.
11. Miura H, Maeda M, Yamamoto N, Yamaoka S. Distinct IkappaB kinase regulation in adult T cell leukemia and HTLV-I-transformed cells. Exp Cell Res. 2005;308:29-40.
12. Dejardin E, Bonizzi G, Bellahcene A, Castronovo V, Merville MP, Bours V. Highly-expressed p100/p52 (NFKB2) sequesters other NF-kappa B-related proteins in the cytoplasm of human breast cancer cells. Oncogene. 1995;11:1835-1841.
13. Lessard L, Begin LR, Gleave ME, Mes-Masson AM, Saad F. Nuclear localization of nuclear factor-kappaB transcription factors in prostate cancer: an immunohistochemical study. Br J Cancer. 2005;93:1019-1023.
14. Chandler NM, Canete JJ, Callery MP. Increased

expression of NF-kappa B subunits in human pancreatic cancer cells. J Surg Res. 2004;118:9-14.

15. Bours V, Dejardin E, Goujon-Letawe F, Merville MP, Castronovo V. The NF-kappa B transcription factor and cancer: high expression of NF-kappa B- and I kappa B-related proteins in tumor cell lines. Biochem Pharmacol. 1994;47:145-149.
16. Annunziata CM, Davis RE, Demchenko Y, et al. Frequent engagement of the classical and alternative NF-kappaB pathways by diverse genetic abnormalities in multiple myeloma. Cancer Cell. 2007;12:115-130.
17. Keats JJ, Fonseca R, Chesi M, et al. Promiscuous mutations activate the noncanonical NF-kappaB pathway in multiple myeloma. Cancer Cell. 2007;12:131-144.
18. Ramakrishnan P, Wang W, Wallach D. Receptor-specific signaling for both the alternative and the canonical NF-kappaB activation pathways by NF-kappaB-inducing kinase. Immunity. 2004;21:477-489.
19. Liao G, Zhang M, Harhaj EW, Sun SC. Regulation of the NF-kappaB-inducing kinase by tumor necrosis factor receptor-associated factor 3-induced degradation. J Biol Chem. 2004;279:26243-26250.
20. Qing G, Qu Z, Xiao G. Stabilization of basally translated NF-kappaB-inducing kinase (NIK) protein functions as a molecular switch of processing of NF-kappaB2 p100. J Biol Chem. 2005;280:40578-40582.
21. Maeda M, Shimizu A, Ikuta K, et al. Origin of human T-lymphotrophic virus I-positive T cell lines in adult T cell leukemia: analysis of T cell receptor gene rearrangement. J Exp Med. 1985;162:2169-2174.
22. Yagi H, Nomura T, Nakamura K, et al. Crucial role of FOXP3 in the development and function of human CD25$^+$CD4$^+$ regulatory T cells. Int Immunol. 2004;16:1643-1656.
23. Sugamura K, Fujii M, Kannagi M, Sakitani M, Takeuchi M, Hinuma Y. Cell surface phenotypes and expression of viral antigens of various human cell lines carrying human T-cell leukemia virus. Int J Cancer. 1984;34:221-228.
24. Foley GE, Lazarus H, Farber S, Uzman BG, Boone BG, McCarthy RE. Continuous cultured human lymphoblasts from peripheral blood of a child with acute leukemia. Cancer. 1965;18:522-529.
25. Weiss A, Wiskocil RL, Stobo JD. The role of T3 surface molecules in the activation of human T cells: a two-stimulus requirement for IL 2 production reflects events occurring at pre-translational level. J Immunol. 1984;133:123-128.
26. Yamaoka S, Courtois G, Bessia C, et al. Complementation cloning of NEMO, a component of the IkappaB kinase complex essential for NF-kappaB activation. Cell. 1998;93:1231-1240.
27. Chinanonwait N, Miura H, Yamamoto N, Yamaoka S. A recessive mutant cell line with a constitutive IkappaB kinase activity. FEBS Lett. 2002;531:553-560.
28. Morita S, Kojima T, Kitamura T. Plat-E: an efficient and stable system for transient packaging of retroviruses. Gene Ther. 2000;7:1063-1066.
29. Yamaoka S, Inoue H, Sakurai M, et al. Constitutive activation of NF-kappa B is essential for transformation of rat fibroblasts by the human T-cell leukemia virus type I Tax protein. EMBO J. 1996;15:873-887.
30. Munoz E, Courtois G, Veschambre P, Jalinot P, Israël A. Tax induces nuclear translocation of NF-kappa B through dissociation of cytoplasmic complexes containing p105 or p100 but does not induce degradation of I kappa B alpha/MAD3. J Virol. 1994;68:8035-8044.
31. Dewan MZ, Terashima K, Taruishi M, et al. Rapid tumor formation of human T-cell leukemia virus type 1-infected cell lines in novel NOD-SCID/γc^{null} mice: suppression by an inhibitor against NF-κB. J Virol. 2003;77:5286-5294.
32. Krappmann D, Emmerich F, Kordes U, Scharschmidt E, Dorken B, Scheidereit C. Molecular mechanisms of constitutive NF-kappaB/Rel activation in Hodgkin/Reed-Sternberg cells. Oncogene. 1999;18:943-953.
33. Wood KM, Roff M, Hay RT. Defective IkappaBalpha in Hodgkin cell lines with constitutively active NF-kappaB. Oncogene. 1998;16:2131-2139.
34. Mori N, Fujii M, Ikeda S, et al. Constitutive activation of NF-kappaB in primary adult T-cell leukemia cells. Blood. 1999;93:2360-2368.
35. Yemelyanov A, Gasparian A, Lindholm P, et al. Effects of IKK inhibitor PS1145 on NF-kappaB function, proliferation, apoptosis and invasion activity in prostate carcinoma cells. Oncogene. 2006;25:387-398.
36. Farina AR, Tacconelli A, Vacca A, Maroder M, Gulino A, Mackay AR. Transcriptional up-regulation of matrix metalloproteinase-9 expression during spontaneous epithelial to neuroblast phenotype conversion by SK-N-SH neuroblastoma cells, involved in enhanced invasivity, depends upon GT-box and nuclear factor kappaB elements. Cell Growth Differ. 1999;10:353-367.
37. Collins T, Read MA, Neish AS, Whitley MZ, Thanos D, Maniatis T. Transcriptional regulation of endothelial cell adhesion molecules: NF-kappa B and cytokine-inducible enhancers. FASEB J. 1995;9:899-909.
38. El-Sabban ME, Merhi RA, Haidar HA, et al. Human T-cell lymphotropic virus type 1-transformed cells induce angiogenesis and establish functional gap junctions with endothelial cells. Blood. 2002;99:3383-3389.
39. Mori N, Sato H, Hayashibara T, et al. Human T-cell leukemia virus type I Tax transactivates the matrix metalloproteinase-9 gene: potential role in mediating adult T-cell leukemia invasiveness. Blood. 2002;99:1341-1349.
40. Hayashibara T, Yamada Y, Onimaru Y, et al. Matrix metalloproteinase-9 and vascular endothelial growth factor: a possible link in adult T-cell leukaemia cell invasion. Br J Haematol. 2002;116:94-102.
41. Fukudome K, Furuse M, Fukuhara N, Orita T, Hinuma Y. Strong induction of ICAM-1 in human T cells transformed by human T-cell leukemia virus type 1 and depression of ICAM-1 or LFA-1 in adult T-cell leukemia-derived cell lines. Int J Cancer. 1992;52:418-427.
42. Mori N, Yamada Y, Ikeda S, et al. Bay 11–7082 inhibits transcription factor NF-kappaB and induces apoptosis of HTLV-I-infected T-cell lines and primary adult T-cell leukemia cells. Blood. 2002;100:1828-1834.
43. Bargou RC, Emmerich F, Krappmann D, et al. Constitutive nuclear factor-kappaB-RelA activation is required for proliferation and survival of Hodgkin's disease tumor cells. J Clin Invest. 1997;100:2961-2969.
44. Yang J, Amiri KI, Burke JR, Schmid JA, Richmond A. BMS-345541 targets inhibitor of kappaB kinase and induces apoptosis in melanoma: involvement of nuclear factor kappaB and mitochondria pathways. Clin Cancer Res. 2006;12:950-960.
45. Gasparian AV, Yao YJ, Kowalczyk D, et al. The role of IKK in constitutive activation of NF-kappaB transcription factor in prostate carcinoma cells. J Cell Sci. 2002;115:141-151.
46. Wang CY, Cusack JC Jr, Liu R, Baldwin AS Jr. Control of inducible chemoresistance: enhanced anti-tumor therapy through increased apoptosis by inhibition of NF-kappaB. Nat Med. 1999;5:412-417.
47. Gilmore TD, Herscovitch M. Inhibitors of NF-kappaB signaling: 785 and counting. Oncogene. 2006;25:6887-6899.
48. Braun T, Carvalho G, Fabre C, Grosjean J, Fenaux P, Kroemer G. Targeting NF-kappaB in hematologic malignancies. Cell Death Differ. 2006;13:748-758.
49. Courtois G, Gilmore TD. Mutations in the NF-kappaB signaling pathway: implications for human disease. Oncogene. 2006;25:6831-6843.
50. Sun SC, Yamaoka S. Activation of NF-kappaB by HTLV-I and implications for cell transformation. Oncogene. 2005;24:5952-5964.
51. Liptay S, Schmid RM, Nabel EG, Nabel GJ. Transcriptional regulation of NF-kappa B2: evidence for kappa B-mediated positive and negative autoregulation. Mol Cell Biol. 1994;14:7695-7703.
52. Bren GD, Solan NJ, Miyoshi H, Pennington KN, Pobst LJ, Paya CV. Transcription of the RelB gene is regulated by NF-kappaB. Oncogene. 2001;20:7722-7733.

A New Humanized Mouse Model of Epstein-Barr Virus Infection That Reproduces Persistent Infection, Lymphoproliferative Disorder, and Cell-Mediated and Humoral Immune Responses

Misako Yajima,[1,a] Ken-Ichi Imadome,[1,a] Atsuko Nakagawa,[2] Satoru Watanabe,[3] Kazuo Terashima,[4] Hiroyuki Nakamura,[1] Mamoru Ito,[6] Norio Shimizu,[3] Mitsuo Honda,[5] Naoki Yamamoto,[4,5] and Shigeyoshi Fujiwara[1]

[1]Department of Infectious Diseases, National Research Institute for Child Health and Development, [2]Pathology Laboratory, Department of Clinical Laboratory Medicine, National Center for Child Health and Development, [3]Department of Virology, Division of Medical Science, Medical Research Institute, and [4]Department of Molecular Virology, Graduate School of Medicine, Tokyo Medical and Dental University, and [5]AIDS Research Center, National Institute of Infectious Diseases, Tokyo, and [6]Central Institute for Experimental Animals, Kawasaki, Japan

The functional human immune system, including T, B, and natural killer lymphocytes, is reconstituted in NOD/Shi-*scid*/IL-2Rγ^{null} (NOG) mice that receive hematopoietic stem cell transplants. Here, we show that these humanized mice can recapitulate key aspects of Epstein-Barr virus (EBV) infection in humans. Inoculation with $\sim 1 \times 10^3$ TD_{50} (50% transforming dose) of EBV caused B cell lymphoproliferative disorder, with histopathological findings and latent EBV gene expression remarkably similar to that in immunocompromised patients. Inoculation with a low dose of virus ($\leqq 1 \times 10^1$ TD_{50}), in contrast, resulted in apparently asymptomatic persistent infection. Levels of activated $CD8^+$ T cells increased dramatically in the peripheral blood of infected mice, and enzyme-linked immunospot assay and flow cytometry demonstrated an EBV-specific T cell response. Immunoglobulin M antibody specific to the EBV-encoded protein BFRF3 was detected in serum from infected mice. The NOG mouse is the most comprehensive small-animal model of EBV infection described to date and should facilitate studies of the pathogenesis, prevention, and treatment of EBV infection.

Epstein-Barr virus (EBV) is a tumor virus associated with a variety of malignancies, including Burkitt lymphoma, nasopharyngeal carcinoma, and Hodgkin lymphoma [1]. It is also an etiological agent of infectious mononucleosis (IM), which is characterized by transient proliferation of EBV-infected B lymphoblastoid cells and an excessive anti-EBV T cell response. EBV has a unique ability to growth transform human B lymphocytes in vitro and establish lymphoblastoid cell lines (LCLs) [2]. EBV-transformed lymphoblasts express 6 nuclear proteins (Epstein-Barr nuclear antigen [EBNA] 1, 2, 3A, 3B, 3C, and LP) and 3 membrane proteins (latent membrane protein [LMP] 1, 2A, and 2B), and this pattern of EBV gene expression is termed latency III. In contrast, Burkitt lymphoma cells express only EBNA1 consistently (latency I), whereas Hodgkin lymphoma and nasopharyngeal carcinoma cells express EBNA1, LMP1, and LMP2 (latency II). In vivo, EBV-transformed cells are effectively removed by virus-specific cytotoxic T cells, and EBV infection in immunocompetent humans is usually subclinical, except for IM caused by primary infection during adolescence or adulthood. However, in immunocompromised hosts, such as patients with AIDS and transplant recipients, EBV-infected B lymphoblasts can proliferate and cause lymphoproliferative disorder.

Received 28 December 2007; accepted 19 March 2008; electronically published 15 July 2008.

Potential conflicts of interest: none reported.

Financial support: Ministry of Health, Labour, and Welfare of Japan (grants H18-Shinko-013 and H19-AIDS-003).

[a] M.Y. and K.-I.I. contributed equally to this study.

Reprints or correspondence: Dr. Shigeyoshi Fujiwara, Dept. of Infectious Diseases, National Research Institute for Child Health and Development, 2-10-1 Okura, Setagaya-ku, Tokyo 157-8535, Japan (shige@nch.go.jp); or, Dr. Norio Shimizu, Dept. of Virology, Div. of Medical Science, Medical Research Institute, Tokyo Medical and Dental University, 1-5-45 Yushima, Bunkyo-ku, Tokyo 113-8519, Japan (nshivir@tmd.ac.jp); or, Dr. Naoki Yamamoto, AIDS Research Center, National Institute of Infectious Diseases, 1-23-1 Toyama, Shinjuku-ku, Tokyo 162-8640, Japan (nyama@nih.go.jp).

The Journal of Infectious Diseases 2008; 198:673–82

0022-1899/2008/19805-0008$15.00
DOI: 10.1086/590502

EBV infects only humans in nature and limited animal species under experimental conditions. It can infect cotton-top tamarins and induce lymphomas, which have been used as a model of EBV-associated lymphomas [3, 4]. Nonhuman primates possess their own lymphocryptoviruses related to EBV, and research on the use of these virus-host systems as models of EBV infection is currently in progress [5, 6]. Small-animal models of EBV have also been developed, which are particularly useful when a large number of animals are necessary. *Scid* mice that receive intraperitoneal transplants of EBV-transformed LCLs or peripheral blood mononuclear cells (PBMCs) isolated from EBV-infected persons develop lymphomas, which have been used as a model of human lymphoproliferative disorder [7–9]. Recently, NOD/*scid* mice transplanted with human hematopoietic stem cells (HSCs) and reconstituted mainly with B lymphocytes were infected with EBV, and the development of lymphoproliferative disorder was described [10]. The immune response to EBV was not studied in these *scid* or NOD/*scid* mouse models. Very recently, a functional human immune system could be reconstituted in highly immunodeficient mouse strains, and these so-called humanized mice were shown able to mount an EBV-specific T cell response [11, 12]. These studies were, however, performed mainly using immunological standpoints and did not provide detailed virological data.

NOD/Shi-*scid*/IL-2Rγ^{null} (referred to here as NOG) is a highly immunodeficient mouse strain that was developed very recently and that, after transplantation with cord blood HSCs, is able to reconstitute most major components of the hematolymphoid system, including T cells, B cells, NK cells, macrophages, and dendritic cells [13–15]. Human T cells that develop in NOG mice are functional in that they can be activated to display cytotoxic activity [15, 16]. These properties made NOG mice an excellent model of human virus infections targeting the immune system, such as those with human T-lymphotropic virus–1 and HIV-1 [17–20]. Here, we provide evidence that humanized NOG mice can reproduce various key aspects of human EBV infection and propose that they may be a valuable tool for studies of EBV infection.

METHODS

Preparation of humanized mice. NOG mice were obtained from the Central Institute for Experimental Animals (Kawasaki, Japan). Protocols for experiments with NOG mice were approved by the Institutional Animal Care and Use Committee of the National Institute of Infectious Diseases (NIID). Cord blood was supplied by the Tokyo Cord Blood Bank after obtaining informed consent. The use of human materials in this research was approved by the institutional review boards of the National Research Institute for Child Health and Development, the NIID, the Tokyo Medical and Dental University, and the Tokyo Cord Blood Bank. The isolation of human CD34$^+$ HSCs from cord blood by means of the MACS Direct CD34 Progenitor Cell Isolation Kit (Miltenyi Biotec), their intravenous injection (1×10^4 to 1.2×10^5 cells/mouse) into 6–10-week-old female NOG mice, and the characterization of the reconstitution of the human hematoimmune system were done as described elsewhere [18, 20]. NOG mice in which the human hematoimmune system was reconstituted are referred here as humanized NOG (hNOG) mice.

Table 1. Primers for reverse-transcription polymerase chain reaction to detect Epstein-Barr virus (EBV) transcripts.

Transcript, primer	Sequence (5'→3')
EBNA1	
5'	gatgagcgtttgggagagctgattctgca
3'	tcctcgtccatggttatcac
EBNA2	
5'	agaggaggtggtaagcggttc
3'	tgacgggtttccaagactatcc
LMP1	
5'	ctctccttctcctcctcttg
3'	caggagggtgatcatcagta
LMP2A	
5'	atgactcatctcaacacata
3'	catgttaggcaaattgcaaa
LMP2B	
5'	cagtgtaatctgcacaaaga
3'	catgttaggcaaattgcaaa
EBER1	
5'	agcacctacgctgccctaga
3'	aaaacatgcggaccaccagc
BZLF1 (first)	
5'	attgcaccttgccgccaccttg
3'	cgcattttctggaagccacccga
BZLF1 (second)	
5'	gaccaagctaccagagtctat
3'	cagaatcgcattcctccagcga
BMRF1	
5'	ctagccgtcctgtccaagtgc
3'	agccaaacagctccttgccca
BLLF1	
5'	gtcagtacaccatccagagcc
3'	ttggtagacagccttcgtatg
GAPDH	
5'	gcctcctgcaccaccaactg
3'	cgacgcctgcttcaccaccctct

NOTE. EBNA, Epstein-Barr nuclear antigen; EBER, EBV-encoded small RNA; LMP, latent membrane protein.

Experimental EBV infection, quantification of viral DNA, and detection of viral mRNAs. Virus production by EBV-infected Akata cells was stimulated by brief treatment with anti-IgG antibody (Dako), and culture fluid was used as inoculum after filtration through a 0.45-μm membrane filter [21]. For virus titration, cord blood lymphocytes were plated at the density

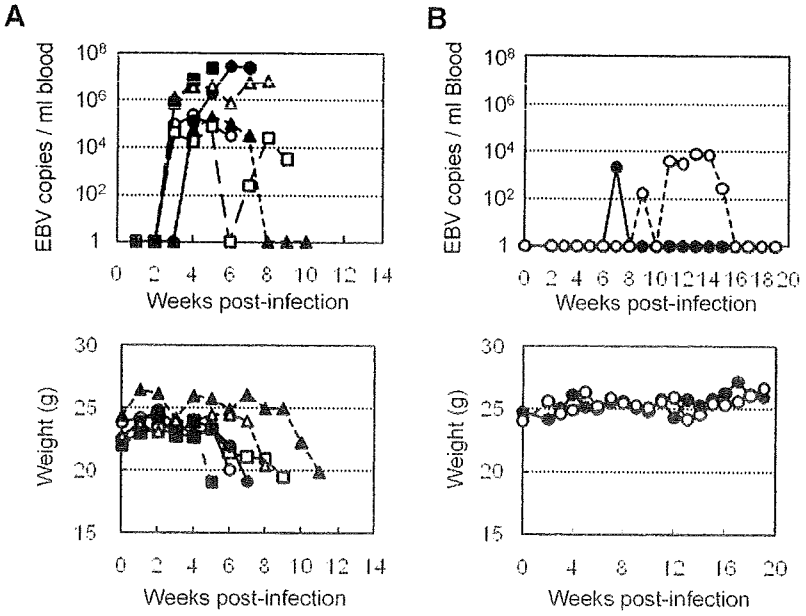

Figure 1. Peripheral blood Epstein-Barr virus (EBV) DNA load and body weight in humanized NOG (hNOG) mice infected with EBV. *A,* Infection at a high dose of virus. Six mice were inoculated intravenously with 1×10^3 TD_{50} of EBV. Peripheral blood EBV DNA load *(upper panels)* and body weight *(lower panels)* were then determined weekly. Each symbol in the graphs represents an individual mouse. Interruption of records indicates the death or killing of a mouse. *B,* Infection at lower doses. Peripheral blood EBV DNA load *(upper panel)* and body weight *(lower panel)* of 2 mice inoculated with low doses of EBV (*black circle,* 1×10^{-1} TD_{50}; *white circle,* 1×10^1 TD_{50}) are shown.

of 2×10^5 cells per well in 6-well plates and then inoculated with serial 10-fold dilutions of virus preparation. The number of wells with proliferating lymphocytes was counted 6 weeks after infection, and the titer of the virus in 50% transforming dose (TD_{50}) was determined by the Reed-Muench method [22]. EBV was inoculated intravenously through the tail vein. EBV DNA was quantified by a real-time quantitative polymerase chain reaction (PCR) assay based on the TaqMan system (Applied Biosystems), as described elsewhere [23]. Analysis of EBV gene expression by reverse-transcription PCR (RT-PCR) was done as described elsewhere, using the primers listed in table 1 [24].

Histopathology, in situ hybridization (ISH), and immunohistochemistry. Tissue samples were fixed in 10% buffered formalin, embedded in paraffin, and stained with hematoxylin-eosin. For phenotypic analysis of proliferating lymphocytes, immunostaining for CD3 (Nichirei), CD4 (Novocastra), CD8 (Nichirei), CD45RO, CD20, CD79a, CD30, Mum1 (Dako), CD23, CD10, CD56 (Novocastra), granzyme B (Dako), and T cell intracellular antigen 1 (Beckman Coulter) was performed on paraffin sections. EBV was detected by immunostaining for LMP1 and EBNA2 (Dako) and by ISH with EBV-encoded small RNA (EBER) probe. Immunohistochemistry and ISH were performed on an automated stainer (Benchmark XT; Ventana Medical Systems), in accordance with the manufacturer's recommendations. To determine the cell lineage of EBV-infected cells, paraffin sections were applied to double staining with EBER ISH and immunohistochemistry.

Detection of EBV-specific T cell response. Enzyme-linked immunospot (ELISPOT) assay was performed with the Immunocyto IFN-γ ELISPOT Kit (MBL), in accordance with the instructions supplied by the manufacturer. Briefly, $CD8^+$ T cells were isolated from PBMCs from EBV-infected hNOG mice with the IMag anti-human CD8 Particles–DM (BD Biosciences). Mixture of these $CD8^+$ T cells and an autologous LCL were incubated with interleukin (IL)–2 in microplates coated with antibody to interferon (IFN)–γ for 17 h. Captured IFN-γ was detected by use of biotinated antibody to IFN-γ and alkaline phosphatase–conjugated streptavidin and was visualized by reaction with the BCIP/NBT chromogen substrate. The unpaired Student's *t* test was used for statistical analysis. IFN-γ secretion in response to EBV was also examined by flow cytometry, as described elsewhere [25]. Briefly, aliquots of murine splenocytes and an LCL were mixed in 6-well plates in the presence of brefeldin A (10 μg/mL) and incubated at 37°C in 5% CO_2 for 17 h. After incubation, the cell suspensions were stained with phycoerythrin-conjugated anti-human CD69, phycoerythrin–Texas red–conjugated anti-human CD45, and phycoerythrin–cyanin 5–conjugated anti-human CD8 for 30 min at 4°C and were fixed with 2% paraformaldehyde. Cells were then permeabilized and stained with BD Perm/Wash buffer (BD Biosciences) containing fluorescein isothiocyanate–conjugated anti-human IFN-γ for 30 min at 4°C. Stained cells were analyzed using an EpicsXL flow cytometer (Beckman Coulter).

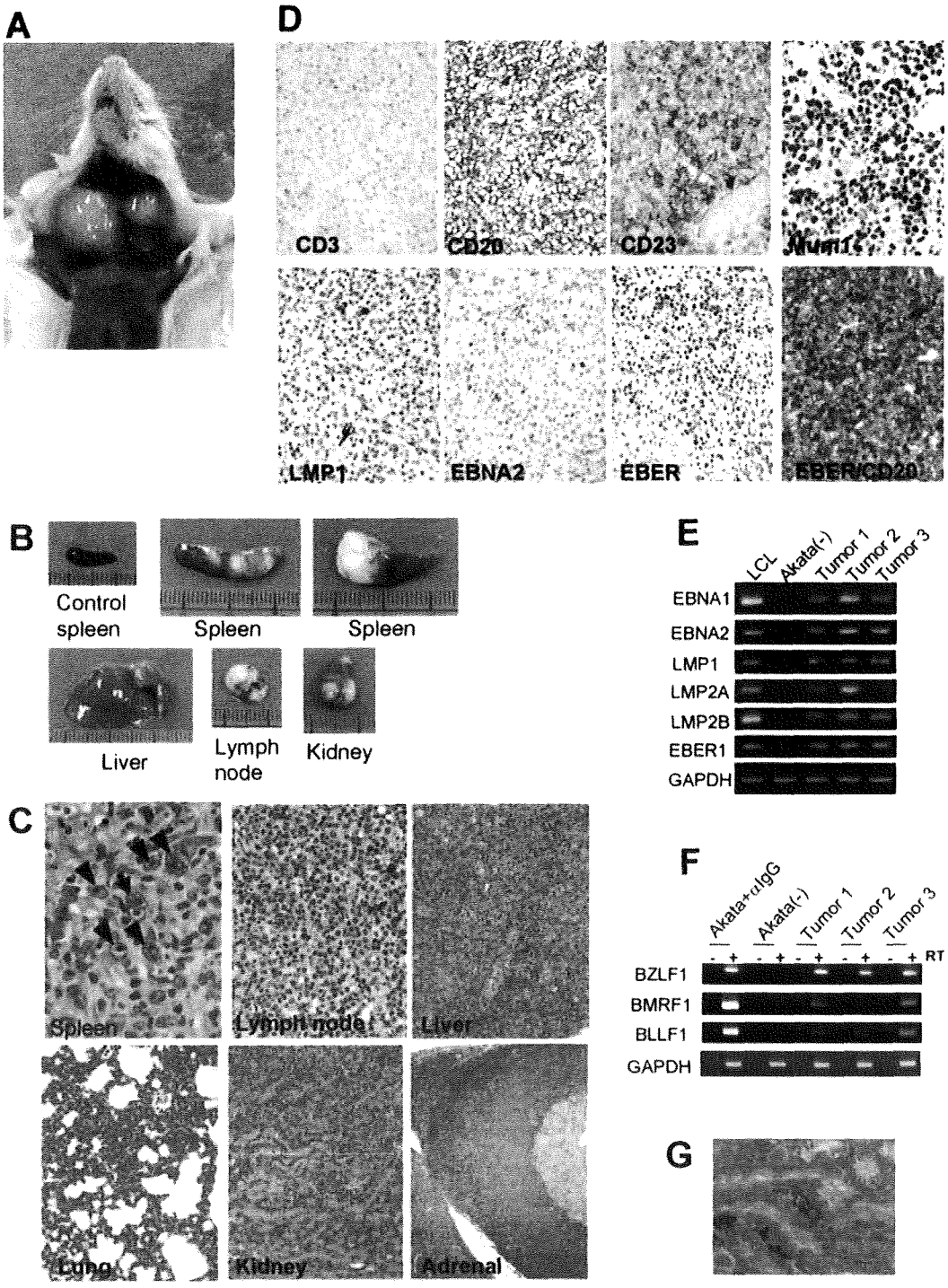

Figure 2. Pathological and virological analyses of Epstein-Barr virus (EBV)–infected humanized NOG (hNOG) mice. *A,* Photograph of an EBV-infected mouse showing tumors in the cervical area. *B,* Photographs of spleens, liver, lymph node, and kidney from EBV-infected mice with lymphoproliferative disorder. The upper left panel shows the spleen from an uninfected mouse. *C,* Photomicrographs of hematoxylin-eosin–stained tissues from mice with lymphoproliferative disorder. The arrow indicates a Reed-Sternberg–like cell, and the arrowheads indicate Hodgkin-like cells. Original magnifications, ×1000 for spleen, ×400 for lymph node, and ×200 for liver, lung, kidney, and adrenal gland. *D,* Immunohistochemical staining for lymphocyte surface markers (CD3, CD20, CD23, and Mum1) and EBV-encoded proteins (latent membrane protein [LMP] 1 and Epstein-Barr nuclear antigen [EBNA] 2), as well as in situ hybridization for EBV-encoded small RNA (EBER), in a lymph node from a mouse with lymphoproliferative disorder. The bottom right panel represents double staining for EBER and CD20. Original magnifications, ×200 for all except EBER/CD20, which is ×400. *E* and *F,* Reverse-transcription polymerase chain reaction detection of latent-cycle *(E)* and lytic-cycle *(F)* EBV gene expression in tumors from EBV-infected hNOG mice. Spleen tumors from 3 different mice were examined for the expression of EBNA1, EBNA2, LMP1, LMP2A, LMP2B, EBER1, BZLF1, BMRF1, and BLLF1. RNA samples from a lymphoblastoid cell line (LCL) *(E)* and anti-IgG–treated Akata cells *(F)* were used as positive controls, and an RNA sample from EBV-negative Akata cells (*E* and *F*) was used as a negative control. Assays were done with (+) or without (−) reverse transcriptase (RT) in panel F. Expression of GAPDH was examined as a reference. *G,* Double staining of EBER and CD20 in the liver of an hNOG mouse that was persistently infected with EBV without developing lymphoproliferative disorder. EBER is stained navy in the nucleus, and CD20 is stained brown in the membrane. Original magnification, ×1000.

Table 2. Quantification of Epstein-Barr virus (EBV) DNA in persistently infected humanized NOG mice.

Organ	Mouse	
	N35-1[a]	N35-3[b]
Bone marrow	ND	4.1×10^4
Spleen	6.2×10^2	5.7×10^3
Liver	ND	2.7×10^4
Lymph node (neck)	1.6×10^3	6.9×10^3
Lymph node (axilla)	ND	2.6×10^2
Lymph node (mesentery)	ND	4.1×10^2
Lungs	2.7×10^3	1.0×10^4
Kidneys	1.2×10^3	4.8×10^4
Adrenal gland	4.4×10^1	8.0×10^5

NOTE. Data are the amounts of EBV DNA measured 22 weeks after infection, in copies per microgram of DNA. ND, not detectable.

[a] Infected at 1×10^{-1} TD_{50}.

[b] Infected at 1×10^1 TD_{50}.

Detection of antibodies specific to EBV. IgM antibody to the EBV BFRF3 protein was detected by immunoblotting essentially as described elsewhere [24], except that horseradish peroxidase–conjugated antibody specific to human IgM (Beckman Coulter) was used as secondary antibody. To prepare the glutathione *s*-transferase (GST)–BFRF3 fusion protein, a DNA fragment spanning the entire coding region of BFRF3 was amplified by PCR (sense primer, 5'-GGCTCGAATTCATGGCACGCCG-GCTGCCC-3'; antisense primer, 5'-GGCTCGGATCCATAC-ACCATGTTTCGTGCCC-3') and inserted to the GST fusion vector pSGENT2, to yield the plasmid pSGENT2-BFRF3. *Escherichia coli* cells harboring pSGENT2-BFRF3 were stimulated with isopropyl β-D-1-thiogalactopyranoside to induce the expression of GST-BFRF3, which was subsequently purified by use of the Bulk GST Purification Module (GE Healthcare).

RESULTS

EBV infection in hNOG mice. Transplantation of human $CD34^+$ HSCs in NOG mice and reconstitution of the human hematoimmune system were done as described elsewhere [18, 20]. In the initial attempts at infection, 1×10^3 TD_{50} of the Akata strain of EBV was inoculated into 6 hNOG mice, and EBV DNA was demonstrated in the peripheral blood of all of them (figure 1*A*). EBV DNA was first evident at 3–4 weeks after inoculation and reached peak levels of $\sim 1 \times 10^6$ EBV DNA copies/μg of DNA. All 6 mice became seriously ill between 5 and 10 weeks after inoculation, with signs of weight loss (figure 1*A*), general inactivity, and piloerection. In contrast, EBV DNA was not detected in the peripheral blood, bone marrow, thymus, spleen, lymph nodes, liver, kidneys, and lungs of 3 control NOG mice that were not transplanted with HSCs but were inoculated with the virus (data not shown). Similarly, no signs of EBV infection were observed in 3 control hNOG mice that were not inoculated with the virus (data not shown). In total, 43 NOG mice that had been humanized with HSCs from 9 different cord blood samples were inoculated with 1×10^3 TD_{50} of EBV, and in 38 of them the results were similar to those observed in the initial 6 mice, with high blood EBV load and severe deterioration in their general condition. Ten of them died and could not be examined further. The remaining 28 mice were killed, and signs of lymphoproliferative disorder were found at autopsy (see the below). These results demonstrate that hNOG mice can be infected with EBV, with a mostly fatal outcome at this virus dose.

EBV-induced lymphoproliferative disorder in hNOG mice. Autopsy of killed mice showed signs of lymphoproliferative disorder typically represented by an overt tumor in the spleen (figure 2*B*). In ~70% (20/28) of the mice autopsied, macroscopical signs of disseminated disease were found in the liver, lymph nodes, or kidneys (figure 2*A* and 2*B*). Seventeen mice were examined pathologically, and 15 of them showed typical histology of diffuse large B cell lymphoma, with remarkable similarity to the human lymphoproliferative disorder in the immunocompromised hosts (figure 2*C*). The tissues contained occasional immunoblasts, Reed-Sternberg–like cells, and Hodgkin-like cells (figure 2*C*). Marked infiltration of large transformed lymphoid cells was also demonstrated in liver, lymph nodes, kidneys, adrenal glands, and lungs (figure 2*C*). Real-time PCR detected high levels ($\sim 1 \times 10^5$ to $\sim 1 \times 10^6$ EBV DNA copies/μg of DNA) of EBV DNA in these organs, and the large transformed lymphoid cells were universally EBV positive by EBER ISH (figure 2*D*). Immunohistochemical analysis showed that the large transformed lymphoid cells were of the activated B cell phenotype, being reactive for CD20 and CD23 and not reactive for CD3 and CD10 (figure 2*D* and data not shown). They were also positive for Mum-1, a late- and postgerminal center cell marker. The EBER-positive cells were CD20-positive B cells (figure 2*D*), and no EBER-positive T cells were identified. Immunostaining revealed that most proliferating cells expressed EBNA2, whereas LMP1 was expressed in only a fraction of them (figure 2*D*). RT-PCR analysis of typical spleen tumors obtained from 3 different mice showed the expression of EBNA1, EBNA2, LMP1, LMP2A, LMP2B; and EBER, consistent with the latency III program of EBV gene expression (figure 2*E*). In addition, transcripts from lytic-cycle EBV genes, including BZLF1 (immediate-early), BMRF1 (early), and BLLF1 (late, encoding gp350/220), were identified (figure 2*F*).

Virus dose–dependent outcome of EBV infection in hNOG mice. To examine the influence of virus dose on the outcome of EBV infection, we inoculated serial dilutions of EBV preparation into 2 lots of hNOG mice, each consisting of 5 mice that had been humanized with the same HSC preparation. Consistent with the results described above, the 4 mice (2 from each lot) that received the higher doses (1×10^3 and 1×10^2 TD_{50}) of the

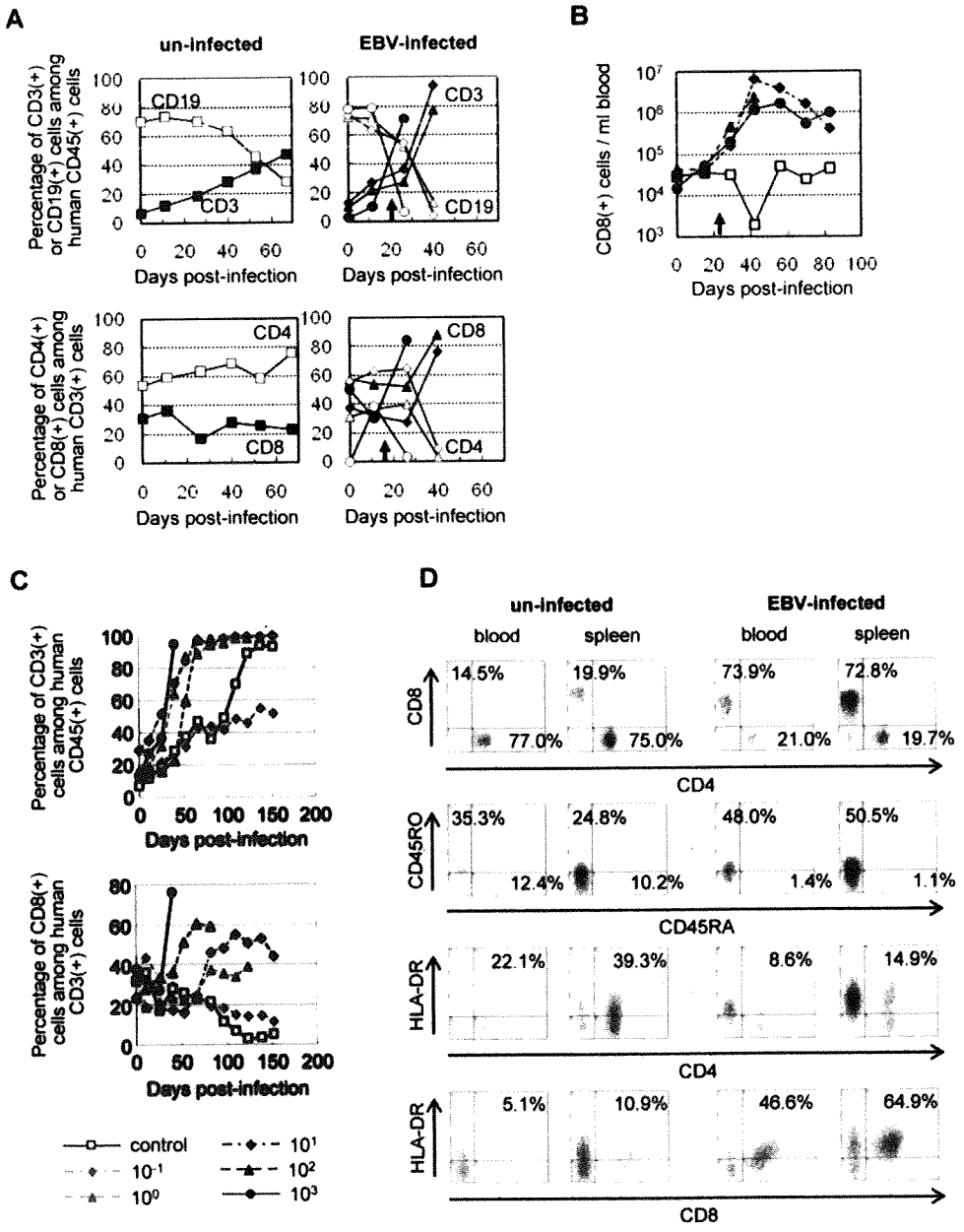

Figure 3. Surface marker expression by peripheral blood T cells in Epstein-Barr virus (EBV)–infected humanized NOG (hNOG) mice. *A,* Changes in the percentages of $CD3^+$ T cells and $CD19^+$ B cells among human $CD45^+$ leukocytes *(upper panels)* and in the percentages of $CD8^+$ cells and $CD4^+$ cells among $CD3^+$ cells *(lower panels)* after infection with EBV. Results obtained from 3 EBV-infected mice and an uninfected mice are shown. White symbols indicate the percentage of $CD19^+$ cells *(upper panels)* or $CD4^+$ cells *(lower panels);* black symbols indicate the percentage of $CD3^+$ cells *(upper panels)* or $CD8^+$ cells *(lower panels).* A vertical arrow in the graph area shows the time point at which EBV DNA was first detected in peripheral blood. *B,* Changes in the no. of $CD8^+$ T cells in the peripheral blood of EBV-infected hNOG mice. White symbols indicate uninfected mice, and black symbols indicate infected mice. Note that cell no. is plotted in a logarithmic scale. *C,* Viral dose–dependent T cell responses in hNOG mice inoculated with serially diluted EBV. Ten-fold serial dilutions of an EBV sample starting from 1×10^3 TD_{50} per inoculate were injected intravenously into NOG mice that had undergone transplantation with the same lot of human hematopoietic stem cells (HSCs). Changes in the percentages of $CD3^+$ T cells among human $CD45^+$ leukocytes *(upper panel)* and in the percentages of $CD8^+$ cells among $CD3^+$ cells *(lower panel)* after inoculation with EBV are shown. The viral dose for each mouse is shown in the key. *D,* Comparison of surface marker expression between EBV-infected mice and control mice. Two mice that underwent transplantation with the same lot of human HSCs were either inoculated with EBV or left uninfected; 10 weeks after inoculation, mononuclear cells obtained from peripheral blood or spleen were gated for the expression of human CD3 and then examined for the expression of CD8 and CD4 *(top panels),* CD45RO and CD45RA *(second from top),* HLA-DR and CD4 *(second from bottom),* and HLA-DR and CD8 *(bottom).*

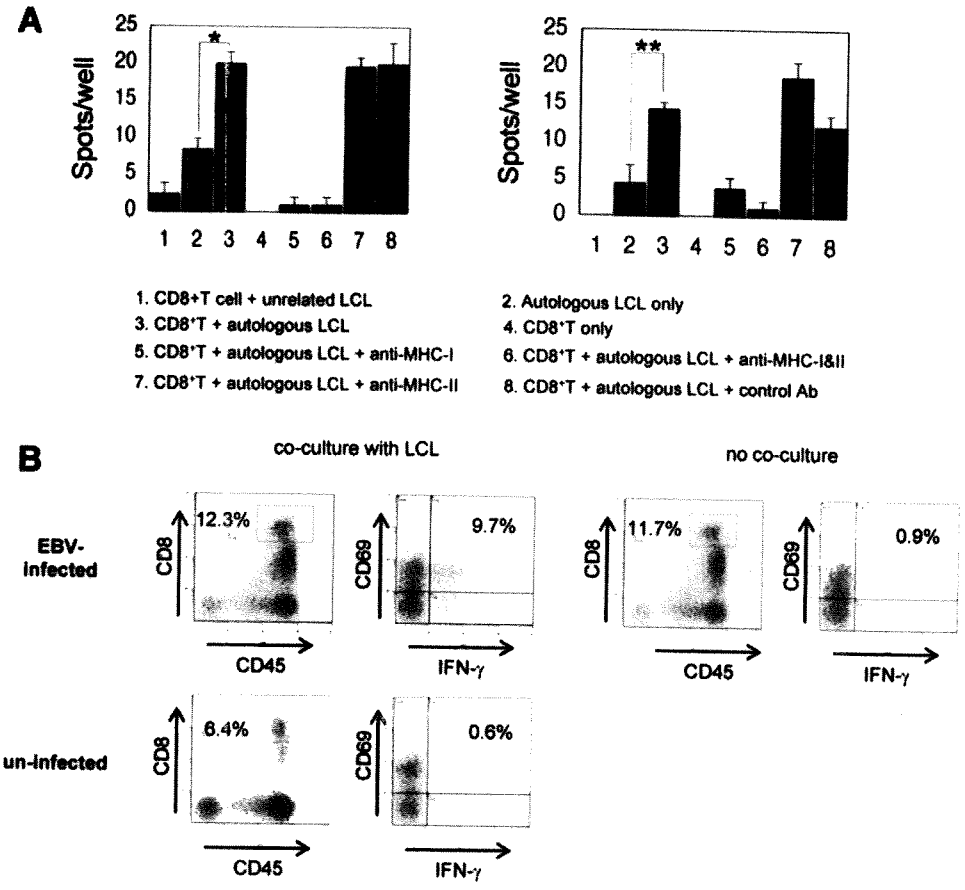

Figure 4. Epstein-Barr virus (EBV)–specific T cell response in humanized NOG (hNOG) mice. *A*, Enzyme-linked immunospot assay for the detection of human T cells producing interferon (IFN)–γ after stimulation with an EBV-positive lymphoblastoid cell line (LCL). $CD8^+$ cells isolated from EBV-infected hNOG mice were cocultured with an autologous LCL, and IFN-γ–secreting cells were counted (3, 5, 6, 7, and 8). To analyze restriction by major histocompatibility complex (MHC), antibody to HLA class I (anti–human HLA-ABC clone W6/32; eBioscience) (5), antibodies to both HLA class I and class II (6), antibody to HLA class II (anti–human HLA-DP,DQ,DR clone CR3/43; Dako) (7), or isotype-matched control antibody (8) were added to the culture. Control experiments included coculture of $CD8^+$ cells with an MHC-mismatched LCL (1), culture of the autologous LCL only (2), and culture of $CD8^+$ cells only (4). Results from 2 infected mice are shown. Five hundred $CD8^+$ cells per well were cultured in the experiment shown on the left, and 250 $CD8^+$ cells per well were cultured in that shown on the right. Spots were counted in triplicate in each of the 8 experimental groups, and the bars represent mean values and SEs. The unpaired Student's *t* test was used for statistical analysis. $^*P < .01$ and $^{**}P < .02$. *B*, Detection of human $CD8^+$ cells that produce IFN-γ in response to stimulation with an EBV-positive LCL by flow cytometry. $CD8^+$ cells were isolated from the spleen of an EBV-infected mouse and cocultured with the autologous LCL. Intracellular IFN-γ was stained and analyzed as described in Methods.

virus died of lymphoproliferative disorder ~5–10 weeks after inoculation. The remaining mice in both of the lots that received lower doses (1×10^1, 1×10^0, and 1×10^{-1} TD_{50}) survived acute infection and appeared normal throughout the observation period of 22 weeks. Although EBV DNA was detected at variable levels in their peripheral blood several weeks after inoculation, it returned to undetectable levels thereafter (figure 1*B*), suggesting that a certain protection mechanism worked to control EBV infection. Importantly, EBV DNA could be still detected in various organs, including spleen, liver, lungs, kidneys, and adrenal glands, at the end of the observation period (22 weeks), indicating that EBV persisted in these mice (table 2). Double staining for EBER and CD20 showed that EBV persisted in B cells (figure 2*G*). Macroscopical examination by autopsy at the end of the observation period did not reveal abnormality in these mice, except for moderate splenomegaly found in a mouse that received 1×10^1 TD_{50}. These results indicate that the outcome of EBV infection in hNOG mice varies with the virus dose; high doses of virus tend to cause fatal lymphoproliferative disorder, whereas lower doses induce apparently asymptomatic persistent infection.

EBV-specific T cell response in hNOG mice. Flow cytometry analysis demonstrated a dramatic increase in the percentage of $CD3^+$ T cells among the human $CD45^+$ leukocytes after infection with EBV. This increase in T cells was accompanied by an increase in the percentage of $CD8^+$ cells among human $CD3^+$ T cells. These changes were seen in virtually all infected mice, and the results from 3 mice are shown in figure 3*A*. The slow increase in the percentage of $CD3^+$ cells in the uninfected mouse represents the process of humanization (i.e., the development of hu-

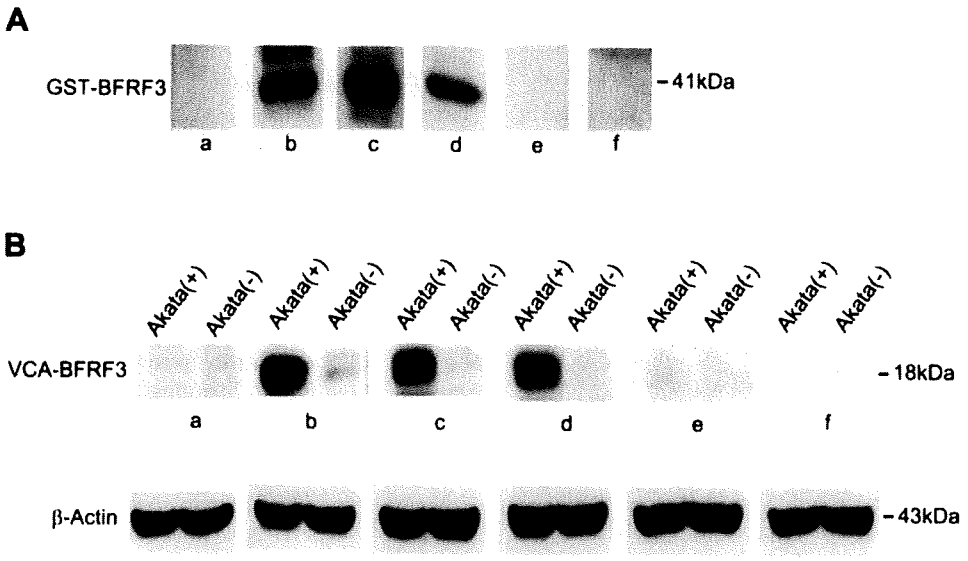

Figure 5. Demonstration of IgM antibody to the Epstein-Barr virus (EBV) BFRF3 protein in the serum of humanized NOG (hNOG) mice. *A*, Immunoblot with the glutathione *s*-transferase (GST)–BFRF3 fusion protein. Purified GST-BFRF3 fusion protein was examined with serum from an EBV-uninfected person *(a)*, an EBV-infected person *(b)*, EBV-infected hNOG mice (*c* and *d*), and an uninfected hNOG mice (*e* and *f*). *B*, Immunoblot with the lysate of EBV-producing Akata cells. Lysate of anti-IgG–treated Akata cells, labeled Akata(+), and of EBV-negative Akata cells, labeled Akata(−), was examined using serum from an EBV-uninfected person *(a)*, an EBV-infected person *(b)*, EBV-infected hNOG mice (*c* and *d*), and uninfected hNOG mice (*e* and *f*).

man T cells). This increase in $CD8^+$ cells were even more conspicuous when their definite number was counted (figure 3*B*). When hNOG mice were inoculated with serially diluted virus samples, a striking dose response was evident; mice inoculated with higher doses exhibited a more profound increase in $CD8^+$ cells at earlier time points (figure 3*C*). Further flow cytometry analyses showed that $CD45RO^+$ memory T cells, compared with $CD45RA^+$ T cells, increased in infected hNOG mice (figure 3*D*). Expression of a T cell activation marker, HLA-DR, was observed mainly in $CD8^+$ cells rather than in $CD4^+$ cells (figure 3*D*).

To demonstrate that these $CD8^+$ T cells were directed against EBV-infected cells, we examined IFN-γ secretion after stimulation with EBV-transformed cells. For this purpose, we first established an LCL using B cells isolated from the same cord blood that was used to isolate HSCs for transplantation. $CD8^+$ T cells, isolated from the peripheral blood of EBV-infected hNOG mice, were incubated with this autologous LCL, and cells secreting IFN-γ were detected by ELISPOT assay. For all 3 EBV-infected hNOG mice (which had been infected at 1×10^3 TD_{50}) thus examined, a significant number of spots were recognized in the wells in which $CD8^+$ T cells were mixed with the autologous LCL, whereas those cells incubated with unrelated LCL had many fewer spots (data from 2 mice are shown in figure 4*A*). $CD8^+$ T cells isolated from uninfected hNOG mice did not give a significant number of spots (data not shown). Release of IFN-γ was blocked by antibody specific to human major histocompatibility complex (MHC) class I but not by that specific to human MHC class II (figure 4*A*). These results clearly show that a T cell response restricted by human MHC class I was mounted against EBV-infected cells. In addition, in 5 of the 6 EBV-infected hNOG mice examined (infected at 1×10^3 TD_{50}), flow cytometry also demonstrated production of IFN-γ by $CD8^+$ T cells isolated from the spleen and stimulated with an autologous LCL (figure 4*B*).

EBV-specific antibody response in hNOG mice. Serum samples from 30 EBV-infected hNOG mice were examined by Western blotting for IgM antibodies reactive with a bacterially expressed GST-BFRF3 fusion protein. The BFRF3 protein is a major component of the virus capsid antigen of EBV [26]. The results are shown in figure 5*A* and indicated that four serum samples (from mice infected at 1×10^1 or 1×10^3 TD_{50}) contained IgM antibody reactive with it. These serum samples reacted also with the 18-kDa BFRF3-encoded protein in the lysate of Akata cells stimulated with IgG antibody to activate virus production (figure 5*B*). Similar experiments with human IgG–specific secondary antibody did not show a positive reaction with either GST-BFRF or $p18^{BFRF3}$. Six serum samples collected from uninfected hNOG mice reacted with neither the 18-kDa protein nor GST-BFRF3 (figure 5 and data not shown). These results indicate that hNOG mice have the ability to mount an IgM response to EBV.

DISCUSSION

The lymphoproliferative disease induced in hNOG mice is remarkably similar to the human lymphoproliferative disorder seen in immunocompromised hosts [27] with respect to histology, surface phenotype, and the type of EBV gene expression

(latency III). Reproduction of latency III in the present study makes for an interesting contrast with the previous model using NOD/*scid* mice, which exhibited the latency II pattern [10].

EBV infection in lower doses resulted in a transient increase in EBV DNA load in the peripheral blood, followed by apparently asymptomatic infection that persisted for at least 22 weeks. This type of asymptomatic EBV infection has not been described in nonprimate models of EBV infection and may be regarded as a model of human EBV latency. To compare this condition in NOG mice with EBV latency in humans precisely, we need to further investigate the nature of host cells (i.e., whether they are memory B cells), the pattern of EBV gene expression in them, and the involvement of anti-EBV immune responses in its maintenance.

In hNOG mice, human T cells develop in thymus tissue, in which epithelial cells are of murine origin [16]. It is therefore interesting that they could mount a T cell response restricted by human MHC class I. Although this suggests that positive selection of human T cells occurred in hNOG mice, the mechanism of T cell education remains unclear. Alloantigen-specific and human MHC class I–restricted T cell cytotoxicity has been reported in hNOG mice [15, 16]. An EBV-induced T cell response was evident in mice that received high doses of virus and developed lymphoproliferative disorder, suggesting that the T cell response in hNOG mice was not sufficient to control EBV-induced lymphoproliferation when they were infected at high doses. That only a minor fraction of $CD8^+$ T cells appeared to be EBV specific, as evidenced by ELISPOT assay and flow cytometry, may explain this result, at least partially. A humoral immune response to EBV has not been documented in previous mouse models of EBV infection, and therefore the NOG mouse may provide a valuable tool to analyze the mechanism and the protective roles of antibody response in EBV infection. We have to date clearly identified only IgM antibody to the 18-kDa component of virus capsid antigen in a minor fraction (4/30) of infected mice. We are currently attempting to improve sensitivity and to see whether hNOG mice can mount a more efficient and divergent antibody response to the virus, possibly including the production of IgG antibodies. Because both the T cell–mediated and the humoral immune response are elicited in hNOG mice, they may be useful in the evaluation of candidate EBV vaccines.

Very recently, humanized mice based on other immunodeficient mouse strains were prepared, and EBV was used as a typical pathogen to analyze their immune functions. Traggiai et al. [12] infected humanized $Rag2^{-/-}IL\text{-}2R\gamma^{-/-}$ mice with EBV and documented an in vitro proliferative response by $CD8^+$ T cells to an autologous LCL. Melkus et al. [11], on the other hand, humanized NOD/*scid* mice by transplanting human fetal liver, thymus, and HSCs and succeeded in inducing an EBV-specific T cell immune response as well as an innate immune response to toxic shock syndrome toxin 1. These 2 studies were performed mainly using immunological standpoints and did not provide detailed data from virological investigations. An advantage of the NOG mouse model described here is that it does not require a fine surgical procedure using human fetal tissue; therefore, NOG mice can be easily provided in large quantities.

In immunocompromised humans, failure of immunosurveillance may lead to the development of lymphoproliferative disorder. We expect that the NOG mouse model can be used to analyze the exact relationship between immunodeficiency and the development of lymphoproliferative disorder. Immune responses in the hNOG mouse can be modulated by immunosuppressive drugs (such as cyclosporine A) or HIV, and the development of lymphoproliferative disorder can be analyzed with special reference to the nature and level of immunodeficiency. This kind of study, which has not been possible with conventional *scid* mice, may reveal an exact condition in which lymphoproliferative disorder develops and may thereby aid the development of a specified immunosuppressive procedure that evades this condition and precludes the risk of lymphoproliferative disorder.

In summary, the NOG mouse is able to recapitulate various essential elements of human EBV infection and is therefore, to our knowledge, the most comprehensive small-animal model of EBV infection described to date. It should be a valuable tool for the study of the pathogenesis, prevention, and treatment of EBV infection.

Acknowledgments

We thank Satoshi Itakura, Fuyuko Kawano, Eri Yamada, Miki Mizukami, and Ken Watanabe for technical assistance. We thank Shizuko Minegishi for advice on flow cytometry, Atsushi Komano for advise on the enzyme-linked immunospot assay, Ayako Demachi-Okamura and Kiyotaka Kuzushima for advice on detection of Epstein-Barr virus–specific T cells, and Shosuke Imai for helpful discussions. We thank the Tokyo Cord Blood Bank for supplying cord blood.

References

1. Rickinson AB, Kieff E. Epstein-Barr virus. In: Knipe DM, Howley PM, eds. Fields virology. Philadelphia: Lippincott Williams & Wilkins, **2001**: 2575–628.
2. Kieff E, Rickinson AB. Epstein-Barr virus and its replication. In: Knipe DM, Howley PM, eds. Fields virology. 4th ed. Philadelphia: Lippincot Williams & Wilkins, **2001**:2511–74.
3. Young LS, Finerty S, Brooks L, Scullion F, Rickinson AB, Morgan AJ. Epstein-Barr virus gene expression in malignant lymphomas induced by experimental virus infection of cottontop tamarins. J Virol **1989**; 63: 1967–74.
4. Miller G, Shope T, Coope D, et al. Lymphoma in cotton-top marmosets after inoculation with Epstein-Barr virus: tumor incidence, histologic spectrum antibody responses, demonstration of viral DNA, and characterization of viruses. J Exp Med **1977**; 145:948–67.
5. Cho Y, Ramer J, Rivailler P, et al. An Epstein-Barr-related herpesvirus from marmoset lymphomas. Proc Natl Acad Sci USA **2001**; 98:1224–9.
6. Moghaddam A, Rosenzweig M, Lee-Parritz D, Annis B, Johnson RP, Wang F. An animal model for acute and persistent Epstein-Barr virus infection. Science **1997**; 276:2030–3.
7. Mosier DE, Gulizia RJ, Baird SM, Wilson DB. Transfer of a functional human immune system to mice with severe combined immunodeficiency. Nature **1988**; 335:256–9.

8. Okano M, Taguchi Y, Nakamine H, et al. Characterization of Epstein-Barr virus-induced lymphoproliferation derived from human peripheral blood mononuclear cells transferred to severe combined immunodeficient mice. Am J Pathol **1990**; 137:517–22.
9. Rowe M, Young LS, Crocker J, Stokes H, Henderson S, Rickinson AB. Epstein-Barr virus (EBV)-associated lymphoproliferative disease in the SCID mouse model: implications for the pathogenesis of EBV-positive lymphomas in man. J Exp Med **1991**; 173:147–58.
10. Islas-Ohlmayer M, Padgett-Thomas A, Domiati-Saad R, et al. Experimental infection of NOD/SCID mice reconstituted with human CD34+ cells with Epstein-Barr virus. J Virol **2004**; 78:13891–900.
11. Melkus MW, Estes JD, Padgett-Thomas A, et al. Humanized mice mount specific adaptive and innate immune responses to EBV and TSST-1. Nat Med **2006**; 12:1316–22.
12. Traggiai E, Chicha L, Mazzucchelli L, et al. Development of a human adaptive immune system in cord blood cell-transplanted mice. Science **2004**; 304:104–7.
13. Hiramatsu H, Nishikomori R, Heike T, et al. Complete reconstitution of human lymphocytes from cord blood CD34+ cells using the NOD/SCID/γ_c^{null} mice model. Blood **2003**; 102:873–80.
14. Ito M, Hiramatsu H, Kobayashi K, et al. NOD/SCID/γ_c^{null} mouse: an excellent recipient mouse model for engraftment of human cells. Blood **2002**; 100:3175–82.
15. Yahata T, Ando K, Nakamura Y, et al. Functional human T lymphocyte development from cord blood CD34+ cells in nonobese diabetic/Shi-scid, IL-2 receptor gamma null mice. J Immunol **2002**; 169:204–9.
16. Ishikawa F, Yasukawa M, Lyons B, et al. Development of functional human blood and immune systems in NOD/SCID/IL2 receptor γ chain^{null} mice. Blood **2005**; 106:1565–73.
17. Miyazato P, Yasunaga J, Taniguchi Y, Koyanagi Y, Mitsuya H, Matsuoka M. De novo human T-cell leukemia virus type 1 infection of human lymphocytes in NOD-SCID, common gamma-chain knockout mice. J Virol **2006**; 80:10683–91.
18. Watanabe S, Terashima K, Ohta S, et al. Hematopoietic stem cell-engrafted NOD/SCID/IL2Rgamma null mice develop human lymphoid systems and induce long-lasting HIV-1 infection with specific humoral immune responses. Blood **2007**; 109:212–8.
19. Dewan MZ, Terashima K, Taruishi M, et al. Rapid tumor formation of human T-cell leukemia virus type 1-infected cell lines in novel NOD-SCID/gammac^{null} mice: suppression by an inhibitor against NF-kappaB. J Virol **2003**; 77:5286–94.
20. Watanabe S, Ohta S, Yajima M, et al. Humanized NOD/SCID/IL2Rγ^{null} mice transplanted with hematopoietic stem cells under nonmyeloablative conditions show prolonged life spans and allow detailed analysis of human immunodeficiency virus type 1 pathogenesis. J Virol **2007**; 81: 13259–64.
21. Takada K, Ono Y. Synchronous and sequential activation of latently infected Epstein-Barr virus genomes. J Virol **1989**; 63:445–9.
22. Condit RC. Principles of virology. In: Knipe DM, Howley PM, eds. Fields virology. Philadelphia: Lippincott Williams & Wilkins, **2001**:19–51.
23. Kimura H, Morita M, Yabuta Y, et al. Quantitative analysis of Epstein-Barr virus load by using a real-time PCR assay. J Clin Microbiol **1999**; 37:132–6.
24. Nakamura H, Iwakiri D, Ono Y, Fujiwara S. Epstein-Barr-virus-infected human T-cell line with a unique pattern of viral-gene expression. Int J Cancer **1998**; 76:587–94.
25. Kuzushima K, Hoshino Y, Fujii K, et al. Rapid determination of Epstein-Barr virus-specific CD8$^+$ T-cell frequencies by flow cytometry. Blood **1999**; 94:3094–100.
26. van Grunsven WM, Nabbe A, Middeldorp JM. Identification and molecular characterization of two diagnostically relevant marker proteins of the Epstein-Barr virus capsid antigen complex. J Med Virol **1993**; 40: 161–9.
27. Rezk SA, Weiss LM. Epstein-Barr virus-associated lymphoproliferative disorders. Hum Pathol **2007**; 38:1293–304.

〔ウイルス　第58巻　第2号，pp.219-220，2008〕

トピックス

2. Sputnik Sweetheart – ウイルスに感染するウイルス

佐藤　佳，小柳義夫

京都大学ウイルス研究所ウイルス病態研究領域

新種の巨大ウイルス「ママウイルス」とそのサテライトウイルス「スプートニク」が，フランス・パリの冷却塔に生息するアメーバから発見された（La Scola et al, *Nature*, 2008）[4]．ママウイルスに寄生するような複製スタイルをとるスプートニクの発見は，これまでのウイルスの定義を再考するきっかけとなるかもしれない．

まず，今回の発見に至るまでの経緯を述べる．APMV（*Acanthamoeba polyphaga* mimivirus）は，現在確認されているウイルスの中で最大径のウイルス種である．その直径は約400 nmであり，マイコプラズマと同等のサイズということからも，その巨大さが窺い知れる．そもそもの発端は，1992年，イングランドで流行した肺炎にある．その原因究明のため，同国各所からサンプルが集められた．その際，ブラッドフォードの冷却塔に生息していたアメーバ中から，グラム陰性菌らしきものが確認された[1]．原核生物の同定に頻用されるrDNA sequencingでもその病原体の正体は明らかにされないまま，11年の月日が流れた．そして2003年，詳細な解析の結果，その細菌らしきものの正体は，なんとウイルスであることが判明したのである[3]．さらにその翌年（2004年），ゲノム解析によって，そのウイルスは1.2 Mbもの直鎖DNAをゲノムとして有していること，1262個の翻訳領域（open reading flame，ORF）を有していることが明らかとなった[5]．そのウイルス粒子の巨大さ，そして保有するゲノムの大きさから，「細菌を模倣しているウイルス（*mi*micking *mi*crobes *virus*）」として，「ミミウイルス（mimivirus）」と名づけられた[2]．

さて，紹介論文[4]のノイエスはふたつある．ひとつめは，APMVの新種「ママウイルス（mamavirus）」が，フランス・パリの冷却塔から新たに見つかったこと．ウイルス粒子のサイズがミミウイルスよりも一回り大きいことから，ママウイルスの発見は，最大のウイルスを更新するものである．そして，ふたつめは，ママウイルスに感染したそのアメーバの中から，まったく別のウイルス様粒子が見つかったことにある．「スプートニク（Sputnik）」というソ連が打ち上げた世界初の無人人工衛星の名を冠されたこのウイルスの直径は50 nmで，約18 kbの環状DNAをゲノムとして持っている．そして，興味深いことに，ママウイルス粒子の中にも，このスプートニク粒子が確認されたのである．さらにスプートニクは，mamavirus factoryと称される，ママウイルス由来のタンパク質から構成されていると考えられる細胞内器官を利用して複製することが，蛍光抗体法による解析から推察された．スプートニクのこの複製スタイルが，細菌におけるバクテリオファージ（bacteriophage）のそれと類似していることから，筆者らは，「スプートニクは，『別のウイルス（ママウイルス）に感染するウイルス』と言えるのではないか」，と述べた上で，バクテリオファージにちなんで，“virophage”という概念を提唱している．

APMV（ミミウイルスとママウイルス）は分類上，nucleocytoplasmic large DNA viruses（NCLDVs）に属しているものの，これまでの「ウイルス」という概念からは遠くかけ離れた特徴をいくつか有している．まず，その粒子の形状である．約400 nmという大きさだけでも驚きだが，さらにこのウイルスは，エンベロープ膜の代わりに，原繊維（fibril）というもので覆われている．また，APMVは1.2 Mbという非常に大きなゲノムを有している．これは，梅毒の原因となる真正細菌*T. pallidum*と同等のゲノムサイズであることからも[1]，その異常な大きさが推察できる．そして，その茫漠なゲノムの中に，1262個もの多種多彩なORFを有していることが確認されている[5]．その

連絡先
〒606-8507
京都大学ウイルス研究所ウイルス病態研究領域
TEL：075-751-4813
FAX：075-751-4812
E-mail：ykoyanag@virus.kyoto-u.ac.jp

ORFの約70%はその塩基配列から機能が予測されており，APMVと同じNCLDVsに分類されるポックスウイルス，種々の細菌類，さらにはほ乳類と相同性のあるORFを複数保有していることが予測されている[5]．そして，特筆すべきは，それらの予測ORFが，tRNA合成酵素，DNA修復酵素，翻訳関連タンパク質，シャペロン分子などもコードしていることである．これはすなわち，リボソーム以外のタンパク質翻訳に必要な分子はほとんど自前で用意していると言っても過言ではない．このことから，APMVは，「リボソームを持たない生物」とも表現できるかもしれない（実際筆者らは，ある総説[6]において，APMVを「キャプシドに包まれた生物と分類すべきである」とも提唱している）．

とは言え，APMVの複製は完全にアメーバに従属しており，これまでの定義からすればやはり，APMVは「ウイルス」の範疇を出ない．さらに，スプートニクも，ママウイルスの複製に従属しているとは言え，ママウイルスはもとよりアメーバなしでは複製することができない．これらのことをふまえると，現在の定義によれば，スプートニクはあくまで，サテライトウイルス（ヘルパーウイルス）に分類されることとなる．

しかしながらウイルスとは，ひとくちに「ウイルス」とカテゴライズされているものの，その形態はもとより，複製様式は枚挙に暇がない．APMVという，これまでの一般的なウイルスのイメージを覆すような巨大ウイルスの発見と，それに「寄生」するかのような小さなサテライトウイルスの発見が，「ウイルス」といういささか広範すぎる枠組みを見つめ直すきっかけとなるかもしれない．

引用文献

1）Birtles RJ, Rowbotham TJ, Storey C, Marrie TJ, Raoult D.: Chlamydia-like obligate parasite of free-living amoebae. Lancet 349, 925-926, 1997.

2）Koonin E V. Virology: Gulliver among the Lilliputians.: Curr Biol 15, R167-169, 2005.

3）La Scola B, Audic S, Robert C, Jungang L, de Lamballerie X, Drancourt M, Birtles R, Claverie J M, Raoult D.: A giant virus in amoebae. Science 299, 2033, 2003.

4）La Scola B, Desnues C, Pagnier I, Robert C, Barrassi L, Fournous G, Merchat M, Suzan-Monti M, Forterre P, Koonin E, Raoult D.: The virophage as a unique parasite of the giant mimivirus. Nature 455, 100-104, 2008.

5）Raoult D, Audic S, Robert C, Abergel C, Renesto P, Ogata H, La Scola B, Suzan M, Claverie J M.: The 1.2-megabase genome sequence of Mimivirus. Science 306, 1344-1350, 2004.

6）Raoult D, Forterre P.: Redefining viruses: lessons from Mimivirus. Nat Rev Microbiol 6, 315-319, 2008.